1987

Interaction of Radiation with Convection in Channel Flows

Yii Hui Wong

Interaction of Radiation with Convection in Channel Flows

By

YII HUI WONG

A thesis submitted
in partial fulfillment of the requirements for the
degree of Master of Science
major in Mechanical Engineering
South Dakota State University
1987

Interaction of Radiation with Convection

in Channel Flows

The thesis is approved as a creditable and independent investigation by a candidate for the degree, Master of Science, and is acceptable for meeting the requirements for this degree. Acceptance of this thesis does not imply that the conclusions reached by the candidate are necessarily the conclusions of the major department.

Dr. A Moutsoglou
Thesis Adviser

Date

Dr. Hassan S. Ghazi
Head, Mechanical
Engineering Department

Date

ABSTRACT

The interaction of convection with radiation in buoyancy induced flow in a channel is re-examined in order to better understand the effects of each flow configuration parameter. The analysis differs from that of Carpenter et al. [4] primarily in the definition of the dimensionless temperature, which is based on the local temperature itself rather than the difference of the local and inlet temperature as chosen in [4]. The present definition avoids the unnecessary complications introduced via the linearization of the radiative terms in [4] which make their interpretation of the presented results rather awkard. The present results concentrate in demonstrating individually the effects of the rate of heat transfer, channel length, channel width, air inlet temperature, and surface emissivities on the temperature of the heated and adiabatic walls respectively.

ACKNOWLEDGEMENTS

My sincere appreciation to Dr. A. Moutsoglou, My thesis adviser, who provided excellent guidance, constant encouragement, and for assistance with the computer programming, Manuscript preparation and for his time which was so freely given.

I remain grateful to Dr. H.S. Ghazi, Head of Mechanical Engineering Department, for his moral and financial support.

My special appreciation is due to my parents for their financial support and encouragement to make my M.S. study possible.

TABLE OF CONTENTS

LIST OF FIGURES

PAGE

NOMENCLATURE

F : shape factor

G : irradiation

Gr_H : modified Grashof number, $g\beta q_{ref}H^4/\nu^2 k$

g : gravitational acceleration

H : Channel width

J : radiosity

k : thermal conductivity

L : length of channel

N : number of elemental surfaces

P : dimensionless pressure

p : pressure

Pr : Prandtl Number

q : local heat flux

R : dimensionless radiation number, $\sigma q_{ref}^3 H^4/k^4$

T : temperature

U, V : dimensionless axial and transverse velocity components

u, v : axial and transverse velocity components

X, Y : dimensionless axial and transverse coordinates

x, y : axial and transverse coordinates

Greek symbol

α : thermal diffusivity

β : coefficient of thermal expansion

ε : surface emissivity

θ : dimensionless temperature, $kT/q_{ref}H$

μ : dynamic viscosity

ν : kinematic viscosity

ρ : density

σ : Stefan-Boltzmann constant

Subscripts

s : surroundings

∞ : ambient

Superscripts

$\bar{}$: mean

$\hat{}$: pertubation

INTRODUCTION

The interaction of radiation and convection in channel flows has been studied for forced convection flows with high surface temperatures [1,2], as well as for natural convection flows [3,4]. The radiation effects were explored by Sparrow et al. [3] for the case of a channel having one isothermal wall and one adiabatic wall. It was found that radiative transport between the heated and adiabatic walls increases the free convective heat transfer considerably. In related applications, such as cooling of electronic equipment and fail-safe decay heat removal systems of breeder reactors, a more appropriate thermal boundary condition is the prescription of surface heat flux rather than temperature. This in effect complicates the computational handling of the radiation-convection interaction. Such a study was reported by Carpenter et al. [4]. However, the choice of the dimensionless parameters used and the coarse linearization employed in [4] makes the presented results very awkward and difficult to interpret. The significant relevance of the phenomenon in recent engineering applications coupled with the shortcomings of the available literature were the incentives for the re-investigation of the problem in the present study.

ANALYSIS

The present study focuses on the interaction of radiation and convection for the natural flow of air in a heated two-dimensional channel. A schematic of the flow configuration and coordinate system is illustrated in Fig. 1. The channel consists of two vertical parallel plates of finite length L, and spaced a distance H apart. An asymmetric non-uniform heat flux is prescribed on the inside of each of the channel walls. The ambient quiescent air surrounding the channel is at a uniform temperature of T_∞. The surfaces enclosing the channel are considered to be large and be at a uniform temperature of T_s. The air is assumed to be a radiatively nonparticipating medium. The dimensionless form of the governing system of equations for steady, two-dimensional laminar free-convection flow in a vertical channel can be written as:

$$\frac{\partial U}{\partial X} + \frac{\partial V}{\partial Y} = 0 \tag{1}$$

$$U\frac{\partial U}{\partial X} + V\frac{\partial V}{\partial Y} = -\frac{d\bar{P}}{dX} + \frac{\partial^2 U}{\partial Y^2} + \theta - \theta_\infty \tag{2}$$

$$U\frac{\partial V}{\partial X} + V\frac{\partial V}{\partial Y} = -\frac{\partial \hat{P}}{\partial Y} + \frac{\partial^2 V}{\partial Y^2} \tag{3}$$

$$U\frac{\partial \theta}{\partial X} + V\frac{\partial \theta}{\partial Y} = \frac{1}{Pr}\frac{\partial^2 \theta}{\partial Y^2} \tag{4}$$

where the Boussinesq approximation was used in modeling the buoyancy term.

The dimensionless parameters appearing in equations (1)-(4) are defined as follows:

$$X = \frac{x}{HGr_H^*}, \qquad Y = \frac{y}{H}, \qquad U = \frac{uH}{\nu Gr_H^*}, \qquad V = \frac{vH}{\nu} \tag{5}$$

$$\bar{P} = \frac{(\bar{p}-p_\infty)H^2}{\rho\nu^2 Gr_H^*}, \qquad P = \frac{pH^2}{\rho\nu^2}, \qquad \theta = \frac{kT}{q_{ref}H}, \qquad \theta_\infty = \frac{kT_\infty}{q_{ref}H}$$

where Gr_H^* is a modified Grashof number based on some reference heat flux, q_{ref}:

$$Gr_H^* = \frac{g\beta q_{ref} H^4}{\nu^2 k} \tag{6}$$

In formulating the governing conservation equations the axial diffusion of momentum and heat was neglected. In addition the longitudinal and lateral pressure gradients were decoupled by representing the local pressure $p(x,y)$ as the sum of a cross-sectional mean pressure $\bar{p}(x)$ that drives the axial flow, and a perturbation about the mean $\hat{p}(x,y)$ which drives the cross-stream flow. In addition the streamwise momentum equation, reflects the local imbalance between the pressure within the channel and the

corresponding hydrostatic pressure $p_\infty(x)$ outside.

The flow boundary conditions are given as:

$$V = 0 \quad \text{at } X = 0\,, \qquad \bar{P} = 0 \quad \text{at } X = 0 \text{ and } X = L/HGr_H^*$$

$$U = V = 0 \quad \text{at } Y = 0 \text{ and } Y = 1 \tag{7}$$

The thermal boundary condition at the inlet of the channel is specified as

$$\theta = \theta_\infty \qquad \text{at} \qquad X = 0 \tag{8}$$

In formulating the thermal boundary conditions at the channel surfaces the energy balance is applied for each discretized element on each surface. Thus, in specifying the condition on the i'th element of the left surface (y=0) in dimensional form, assuming graybody behavior, one gets:

$$q_i\Big|_{y=0} = -k\frac{\partial T_i}{\partial y}\Big|_{y=0} + \varepsilon_i \sigma T_i^4\Big|_{y=0} - \varepsilon_i \sum_{m=1}^{N} J_m F_{i-m}$$

$$- \varepsilon_i F_{i\text{-top}} \sigma T_s^4 - \varepsilon_i F_{i\text{-bot}} \sigma T_s^4 \qquad \text{at } y = 0 \tag{9}$$

where q_i is the prescribed local heat flux on element i, and N is the number of elemental surfaces on the opposing surface (y=H). The last two terms signify the contribution of the surroundings, radiating through the inlet and exit of the channel. In order to express the radiosities J_m of the elemental surfaces contributing to the irradiation in equation (9), an energy balance is invoked for each elemental surface on the opposite surface at y=H:

$$q_m\Big|_{y=H} = k\frac{\partial T_m}{\partial y}\Big|_{y=H} + \varepsilon_m \sigma T_m^4\Big|_{y=H} - \varepsilon_m G_m \qquad (10)$$

at y = H for m = 1, 2, ... , N.

Since the surfaces on the channel are also opaque, equation (10) can be rewritten as:

$$q_m\Big|_{y=H} = k\frac{\partial T_m}{\partial y}\Big|_{y=H} + J_m - G_m \qquad (11)$$

at y = H for m = 1, 2, ... , N.

Eliminating the irradiation and solving for the radiosity J_m from equations (10) and (11), and substituting for J_m into equation (9) results in dimensionless form:

$$\left.\frac{q_i}{q_{ref}}\right|_{Y=0} = -\left.\frac{\partial\theta_i}{\partial Y}\right|_{Y=0} + \left.\varepsilon_i R\theta_i^4\right|_{Y=0} - \varepsilon_i \sum_{m=1}^{N} F_{i-m}\left[\frac{(1-\varepsilon_m)}{e_m}\left(\left.\frac{\partial\theta_m}{\partial Y}\right|_{Y=1}\right.\right. \tag{12}$$

$$\left.\left. - \left.\frac{q_m}{q_{ref}}\right|_{Y=1}\right) + \left.R\theta_m^4\right|_{Y=1}\right] - \varepsilon_i F_{i\text{-top}} R\theta_\infty^4 - \varepsilon_i F_{i\text{-bot}} R\theta_\infty^4$$

at $Y = 0$ for $i = 1, 2, \ldots, N$.

Similarly, for the right wall:

$$\left.\frac{q_j}{q_{ref}}\right|_{Y=1} = \left.\frac{\partial\theta_j}{\partial Y}\right|_{Y=1} + \left.\varepsilon_j R\theta_j^4\right|_{Y=1} - \varepsilon_j \sum_{n=1}^{N}{}' F_{j-n}\left[\frac{(1-\varepsilon_n)}{\varepsilon_n}\left(-\left.\frac{\partial\theta_n}{\partial Y}\right|_{Y=0}\right.\right. \tag{13}$$

$$\left.\left. - \left.\frac{q_n}{q_{ref}}\right|_{Y=0}\right) + \left.R\theta_n^4\right|_{Y=0}\right] - \varepsilon_j F_{j\text{-top}} R\theta_\infty^4 - \varepsilon_j F_{j\text{-bot}} R\theta_\infty^4$$

at $Y = 1$ for $j = 1, 2, \ldots, N$.

where the surroundings temperature was assumed to be that of the quiescent ambient air T_∞, and the radiation number R is defined as:

$$R = \frac{\sigma q_{ref}^3 H^4}{k^4} \tag{14}$$

The shape factors, F, appearing in equations (12) and (13) are evaluated systematically via a combination of Hottel's rule of crossed and uncrossed strings and the decomposition rule.

The governing system of differential equations (1)-(4), and boundary conditions (7), (8), (12) and (13) are characterized by the following dimensionless parameters: The aspect ratio L/H, the modified Grashof number, Gr_H, the dimensionless inlet temperature θ_∞, the dimensionless heat fluxes on the left and right channel walls, the Prandtl number Pr, the radiation number R, and the emissivities of the left and right surfaces. An additional dimensionless parameter $\theta_s = kT_s/q_{ref}H$ must be assigned when the surroundings surface temperature is different than that of the ambient air.

The number of dimensionless parameters in this study exceeds the corresponding number in the study of Carpenter et al. [4] by one. Specifically, the inlet temperature characterized by θ_∞ above, is not a direct required input in [4]. This is due to the difference in the definition of the dimensionless temperature θ, where it is based on the temperature difference $T-T_\infty$ in [4] rather then on T itself, as can be seen from equation (5), in this study. The definition of θ based on $T-T_\infty$ which is the appropriate choice for pure convective flows introduces complications in the linearization of the radiative term. Thus, the linearization used in [4] results in requiring the estimation of an "average absolute surface-ambient temperature" defined in that study for the usability of the presented results. In the present study the choice in defining θ as in equation

(5) not only accounts directly for the effect of the ambient temperature but also lacks any of the ill-effects of the linearization observed in [4].

COMPUTATIONAL PROCEDURE

Despite the parabolization of the governing differential equations described in the previous section, the system of equations is inherently elliptic via the boundary conditions. Whereas in pure free-convection problems the ellipticity is due to the fact that the inlet velocity is unknown while the pressure imbalance has to vanish at both the inlet and exit of the channel, in the combined convection-radiation problem the radiative terms in the thermal boundary condition, equations (12)-(13), are additionally elliptic in nature.

The streamwise momentum and energy equations, (2) and (4), were solved by utilizing a control volume suggested by Patankar and Spalding [5] tailored for parabolic equations, while adopting the finite-difference procedure of Patankar [6] that employs the power law scheme for treating the convection-diffusion terms. A Newton-Raphson iterative method suggested by Raithby and Schneider [7] was utilized in computing the axial mean pressure gradient from the requirement of overall mass conservation at each streamwise location as the solution marched downstream. The transverse momentum equation (3) was solved at each cross-stream plane using the Simpler algorithm of Patankar [5], with the control volumes staggered in the transverse direction. The transverse velocities were computed by imposing the continuity constraint. Each set of resultant algebraic equations was solved using the Tridiagonal Matrix Algorithm of Thomas.

The computational scheme in addition to invoking the standard local iterations at each streamwise location associated with the Patankar-Spalding and Patankar schemes, it also required two global iterations on account of the two aforementioned causes for ellipticity. The unknown steamwise velocity at the inlet of the channel was assumed to be uniform and its value was determined by Newton-Raphson iteration scheme from the constraint that the mean pressure imbalance vanishes at the exit of the channel. A Gauss-Seidel iterative scheme was employed for handling the radiative terms in the thermal boundary conditions. Consequently, the procedure only required the linearization of just the second term on the right-hand side of equations (12) and (13). This was achieved by employing a Taylor series type of linearization:

$$\theta^4 \simeq \theta^{*4} + 4\theta^{*3}(\theta - \theta^*) \qquad (15)$$

where θ^* is the previous iterative value of the wall temperature. The remaining terms that involve temperatures raised to the fourth power were left as they are and evaluated from their current iterative values.

Forty-three grid points were deployed in the transverse direction while 20 rows of grid points were selected in the streamwise direction. The streamwise grid points were positioned at equal distance apart with the first and last row of points situated at the inlet and exit planes of the channel. In generating the transverse mesh, the control-volume boundaries were drawn first,

while the grid points were placed at the centers of the control volumes. The first and last transverse grid point as well as the first and last control-volume boundary were located respectively on the left and right channel walls. The width of the first and last control volume was half of those in between. In estimating the shape factors, the length of each of the 20 elemental surfaces on each wall, along which the temperature was governed by the local grid temperature, was chosen to be the streamwise grid spacing except for the first and last surfaces. The first element had a length of one-and-a half the streamwise grid spacing that included the first two grid points, with its temperature being governed by the second grid, as the first grid was situated at the inlet plane. The last element, N=20, had a length of half the streamwise grid spacing since for the rest of the elements the grids were positioned at the centers of each. Tests with 41 rows of grid points with 83 transverse grids in each row produced results that differed by only less than 1% from the chosen mesh of 21 rows by 43 transverse grids.

RESULTS

The primary concern of the current study is the assessment of the degree of contribution of radiation in altering the channel wall temperatures. Even though the analysis can be carried out for arbitrarily prescribed heat fluxes on each of the walls, the present results concentrate on the case studied in [4]: a channel where one surface is heated uniformly while the other is kept insulated. With the reference heat flux chosen as the prescribed uniform flux, one symbolically has:

$$\frac{q}{q_{ref}} = 1 \text{ at } Y = 0 \quad , \qquad \frac{q}{q_{ref}} = 0 \text{ at } Y = 1 \tag{16}$$

for input into equations (12) and (13) respectively.

With the left and right heat fluxes prescribed by equation (16), the four governing dimensionless parameters L/H, Gr_H^*, θ_∞ and R, are functions of only four physical dimensional variables, if one excludes the surfaces emissivities and the thermophysical properties of the fluid which are functions of some average temperature. These four are the channel length L, channel width H, fluid inlet temperature T_∞, and the prescribed uniform heat flux on the heated left surface, q_{ref}. The parametric study is thus concerned with the independent effects of each of these four dimensional variables on the heated and adiabatic wall temperatures. In estimating the corresponding dimensionless parameters for use in

the solution algorithm, the thermophysical properties of the fluid are evaluated at the inlet temperature. In the figures that follow, the dimensional physical variables with their appropriate units rather than the dimensionless parameters are chosen to be depicted. Whenever appropriate, the "combined" convection-radiation results are compared in the figures to those for pure free-convection, which are obtained by replacing the thermal boundary condition equations (12) and (13) by:

$$\left.\frac{q_i}{q_{ref}}\right|_{Y=0} = -\left.\frac{\partial\theta_i}{\partial Y}\right|_{Y=0} , \qquad \left.\frac{q_j}{q_{ref}}\right|_{Y=1} = \left.\frac{\partial\theta_j}{\partial Y}\right|_{Y=1} \tag{17}$$

$$\text{for } i, j = 1, 2, \ \ldots \ , N$$

in conjunction with equation (16).

The effects of the combined radiation-convection interaction on the channel wall temperatures are shown for three heat fluxes in Figs.2 and 3. The net radiation transfer from the heated to the adiabatic wall induces as expected a reduction in the temperature of the heated wall (Fig.2), while elevating the adiabatic wall temperature (Fig.3) when compared to corresponding temperatures for pure free-convection indicated by dotted lines. While the maximum temperature for the pure free-convection case occurs always at the exit of the channel, the maximum temperature for the combined interaction case occurs around x/L = 0.9 for both surfaces for the specified conditions in the two figures. It is the net radiation loss

from the exit walls to the much colder surroundings that shifts the maximum temperature upstream in the channel, and causes the hump seen in the graphs. The radiation-associated drop and elevation of the heated and adiabatic walls respectively, are of the same order. For instance, the percent reduction of the heated wall temperature due to radiation at mid-channel, x/L = 0.5, is about 11.48% for q_{ref} = 750 W/m^2, 8.28% for 500 W/m^2 and 2.0% for 100 W/m^2. The corresponding elevation of the adiabatic wall temperature is respectively 13.66%, 9.64% and 2.14%.

The transverse variation of the air temperature in the channel is plotted in Fig. 4 at streamwise locations near the inlet, mid-channel, and exit. For pure free-convection the minimum temperature of the air always occurs at the adiabatic wall, y/H = 1. When radiation is accounted for, the minimum shifts very close to the center of the channel y/H = 0.5, for all streamwise locations. The net radiation transfer from the heated to the adiabatic wall and the associated reduction of the heated wall temperature results in a reduction of the convective heat transfer to the fluid from the heated wall, as evidenced by the reduction of slope at y/H = 0. On the other hand the respective elevation of the adiabatic wall temperature induces a convective flux at y/H = 1 that transfers the net radiation gain to the fluid via convection. The overall effect of the redistribution of the energy at each streamwise location is to bring the temperature of the two walls closer together and tend to make the channel fluid isothermal. A very interesting trend is observed at the adiabatic wall at the exit of the channel, where the

temperature slope approaches zero for the combined mode. This is due to considerable radiative loss from the exit to the colder surroundings. This, eventually at larger q_{ref} values, will make the fluid at the exit near the adiabatic wall hotter than the wall itself, that will cause buoyancy induced downwash velocities that invalidate the parabolicity of the conservation equations and will result in the non-convergence of the solution algorithm. For the specified conditions in Fig. 4 the modified Grashof number as defined by equation (6) is of the order of $Gr_H^* = 36895$ that is still in the laminar regime.

To demonstrate the relative significance of the convection and radiation contribution to the total net heat flux, the streamwise variation of the net radiative flux leaving each surface is plotted respectively in Figs. 5 and 6 for the heated and adiabatic walls. It is noted that the first term on the right-hand side of equations (12) and (13) represents the respective net convective flux from the wall to the fluid, while the remaining terms on the right-hand side of each equation signify the net radiative flux leaving each surface. The convective and radiative heat fluxes are non-dimensionalized with respect to the total net heat flux prescribed on the heated wall at each streamwise location. For the conditions specified by equation (16) the total net heat is represented by q_{ref}. Thus, the corresponding convective flux from the heated wall may be inferred by simply subtracting from unity the radiative distribution indicated in Fig.5. On the other hand, the respective convective flux from the adiabatic wall is equal in magnitude and opposite in sign to the

radiative distribution indicated in Fig. 6. As observed from Figs.5 and 6 the net radiative transfer remains constant throughout most of the channel except near the inlet and primarily the exit. For the specified conditions this constant ranges for both walls from 35 to 40 percent of the prescribed total flux, as the flux varies from 100 to 750 W/m^2. An inspection of the two figures reveals that in the majority of the channel excluding the exit, the net radiative transfer from the heated wall to the adiabatic wall is primarily between two directly opposing area segments as the net radiative loss of the heated wall is approximately equal to the net radiative gain of the adiabatic wall at each streamwise location. This is due to the smallness of the specified width of the channel, H = 0.01 m, that makes the shape factors between opposing segments close to unity. In addition, the adjacent surfaces that do participate in the radiation transfer are of comparable temperatures and thus do not contribute to the net flux significantly. This is not the case, however, near the channel exit where the end segments are in radiative communication with the colder surroundings that are considered to be at the inlet air temperature. As a result the net radiative loss from the last wall segment of the heated wall increases sharply (Fig.5) as most of it goes to the surroundings with an associated decrease in the magnitude of the net radiative gain of the adiabatic wall (Fig.6).

The effects of the radiation exchange on the average air velocity and subsequently on the air flow rate are depicted in Fig.7, where the inlet velocity, assumed uniform as a priori, is plotted as a function of the prescribed flux on the heated wall. The

corresponding volumetric flow rate per unit depth of the channel can be easily deduced by multiplying the value of the inlet velocity by the appropriate channel width H, for the cases illustrated in Fig.7. The net radiation transfer from the heated to the adiabatic wall and the subsequent convection transfer from the adiabatic wall to the fluid may cause significant increases in the average velocity and thus flow rate over those for pure free convection. As can be seen from the figure these increases magnify with increasing channel width. Thus for q_{ref} = 750 W/m^2, L = 1 m, H = 0.02 m the increase on the average velocity due to radiation is about 42%.

The transverse velocity profiles of the air in the channel for three streamwise locations corresponding to those in Fig.4, are plotted in Fig.8. As the net radiation transfer tends to bring the temperatures of the two walls closer at each streamwise location, the skewness of the free-convection velocity profiles diminishes and a more parabolic type shape prevails. This also seems to accelerate the hydrodynamic development of the velocity profiles as can be attested from the figure.

The streamwise variation of the bulk temperature of the air is depicted in Fig. 9. Due to the net radiative losses to the cooler surroundings the total energy transfer to the air is less than the corresponding case for free-convection. This results in a decrease in the local value of the air bulk temperature when compared to that for free convection. The deviation increases as the channel exit is approached. As expected, the reduction in the bulk temperature due to radiation becomes more significant with increasing channel width as

observed from the figure.

The effects of the length of the channel on the temperature of the heated and adiabatic walls are indicated respectively in Figs. 10 and 11. As larger average velocities persist with longer channels an approprite reduction in the temperature of the walls is experienced with length, as observed from the two figures. The magnitude of this reduction seems to be not strongly dependent on the convection-radiation interaction for either wall.

Figures 12 and 13 portray the effects of the channel width on the heated and adiabatic wall temperatures respectively. As seen from Fig. 12, the variation of the heated wall temperature with the channel width becomes pronounced primarily in the latter part of the channel. For the adiabatic wall in Fig. 13, the presence of the radiation seems to reduce the significance of the channel width on the adiabatic wall temperature.

The effects of the emissivities on the two wall temperatures are illustrated in Figs. 14 and 15, respectively. As expected the effect of radiation on both wall temperatures diminishes with decreasing emissivities. When the emissivities of the heated and adiabatic walls are interchanged the temperature for either wall is only affected near the exit of the channel due to the radiative losses to the cooler surroundings.

In Figs 16 and 17 the inlet temperature effects on the heated and adiabatic wall temperatures are respectively depicted. As can be observed from the two figures the relative shift in the wall temperatures due to the presence of radiation seems to be insensitive

to the inlet air temperature for the specified conditions.

The present results are compared with the experimental data of Carpenter et al. [4] in Fig.18. As the authors were unable to infer directly from [4] the dimensional configuration parameters for which the data was obtained, the comparison was based only on matching the indicated channel aspect ratio and surface emissivities. Thus, in Fig.18, the present computational results are for a channel with a length of L=0.1 m and width H=0.01 m, with surface emissivities of either 0.995 or 0.05. The figure illustrates the variation of a dimensionless maximum temperature for the heated and adiabatic walls respectively as a function of an average Grashof number defined in [4]. As expected, despite the ambiguity of the compared channel configuration, when raidation is not significant, $\varepsilon_h = \varepsilon_a = 0.05$, there is excellent agreement between the predicted and experiemental data, as long as the aspect ratio is the same. When radiation is present, $\varepsilon_h = \varepsilon_a = 0.995$, the deviation between the presentand experimental results must be due to the difference in the channel configuration assumed for the sake of comparison for the present results and that used in [4] for obtaining the empirical data.

Finally, Fig. 19 exhibits the effect of placing a shield in the middle of a channel heated uniformly at the same rate on both sides. As attested from the figure, when there is no shield in the channel which is heated uniformly on both sides (H=0.02 m), the radiation effect is negated by the symmetry in the channel and it only manifests its presence near the exit of the channel due to the

radiative loss to the surroundings. When a shield is placed in the middle of the same uniformly heated channel, making the channel width in each half H=0.01 m, the net radiation exchange between each of the heated walls and the shield, induces the reduction in the heated wall temperature shown in Fig. 19.

SUMMARY

An assessment of the effects of the uniform rate of heat transfer, channel length, channel width, inlet air temperature and surface emissivities on the radiation-associated respective reduction of the heated wall temperature and elevation of the adiabatic wall temperature is presented.

The redistribution of the supplied energy of the heated wall due to radiation tends to bring the temperatures of the heated and adiabatic walls closer together. For the specified conditions the magnitude of the net radiative transfer remains approximately the same in the majority of the channel except near the inlet and exit where radiation with the surroundings could be quite important. Considerable increases in the average velocity may occur due to radiation over those for pure free convection. Finally, significant decreases in the wall temperatures of a symmetrically heated channel may be achieved by placing a shield in the middle of the channel that activates the otherwise absent radiation mode.

RECOMMENDATIONS

The study was concerned with the interaction of free convection and radiation in laminar, two-dimensional flow in a channel. Extensions of the present study may be foreseen in the following areas:

1. At larger heating rates or channel widths the downwash velocities that may be induced due to radiation near the exit of the adiabatic wall will require the solution of the fully elliptic Navier-Stokes equations.

2. At larger heating rates or channel widths the flow will eventually become turbulent in nature. A mixing length model may be incorporated to account for the resultant turbulent eddy viscosity and eddy diffusivity.

3. For finite depth channels the three dimensional effects will become significant and require the consideration of the 3-D Navier-Stakes equations.

4. Finally, some experiments may be conducted for comparison with the computationally predicted results.

REFERENCES

1. E. G. Keshock, R. Siegel, Combined radiation and convection in an asymmetrically heated parallel plate flow channel, Trans.Am.Soc.Mech.Engrs,Series C,J.Heat Transfer, **86,** 341-350(1964).

2. S. T. Liu, and R. S. Thorsen, Combined forced convection and radiation heat transfer in asymmetrically heated parallel plates, Proc. Heat Transfer and Fluid Mechanics Inst., Stanford University Press, Palo Alto, CA, 32-44(1970).

3. E. M. Sparrow, S. Shah, and C. Prakash, Natural convection in a vertical channel: I. Interacting convection and radiation. II. The vertical plate with and without shrouding, Numer. Heat Transfer **3,** 297-314(1980).

4. J. R. Carpenter, D. G. Briggs, and V. Sernas, Combined radiation and developing laminar free convection between vertical flat plates with asymmetric heating, J. Heat Transfer **98,** 95-100(1976)

5. S. V. Patankar, and D. B. Spalding, A calculation proceduce for heat, mass, and momentum transfer in three-dimensional parabolic flows, Int. J. Heat and Mass Transfer **15,** 1787-1806(1972).

6. S. V. Patankar, Numerical Heat Transfer and Fluid Flow. Hemisphere, Washington, DC (1980).

7. G. D. Raithby, and G. E. Schneider, Numerical solution of problems in incompressible fluid flow: treatment of the velocity-pressure coupling, Numer. Heat Transfer **2,** 417-440(1979).

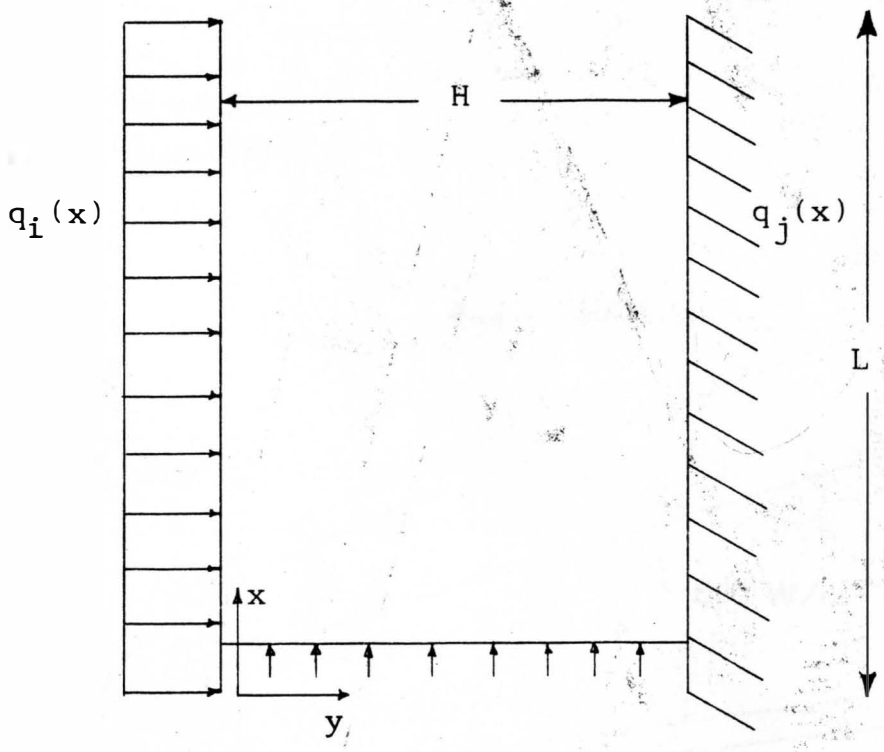

Fig. 1 Flow schematic and coordinate system.

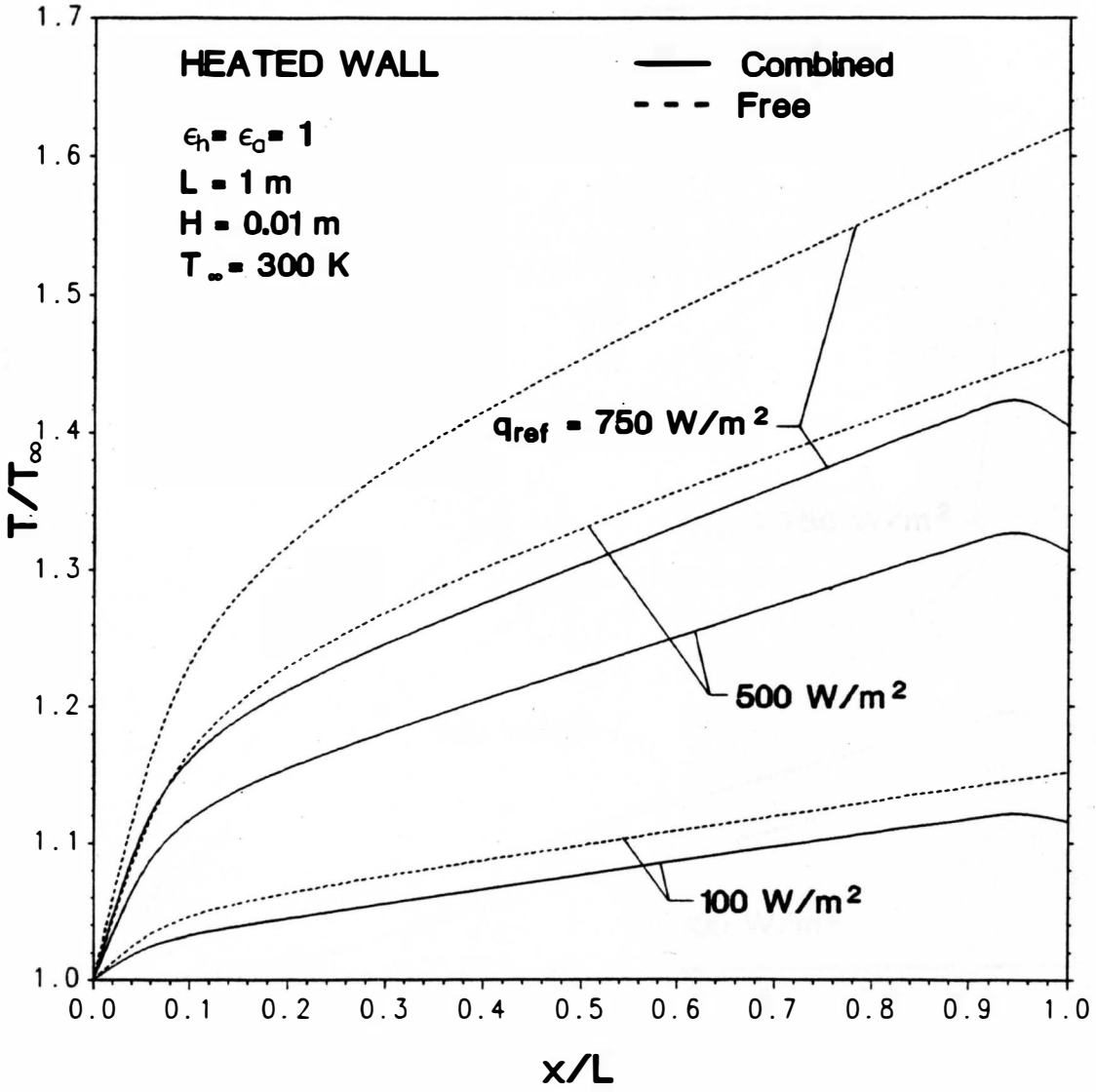

Fig. 2 Effect of rate of heat flux on the heated wall temperature.

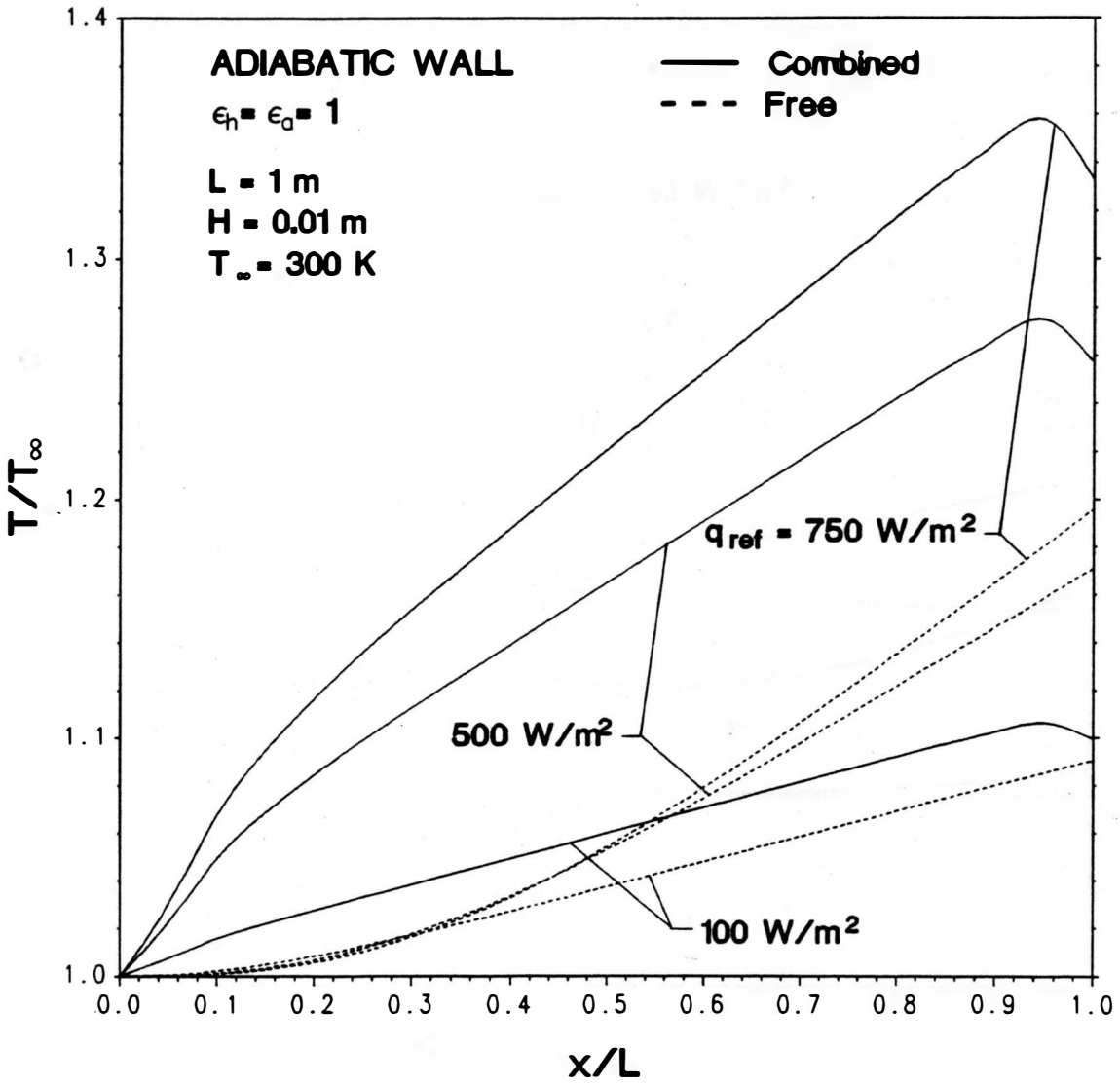

Fig. 3 Effect of rate of heat flux on the adiabatic wall temperature.

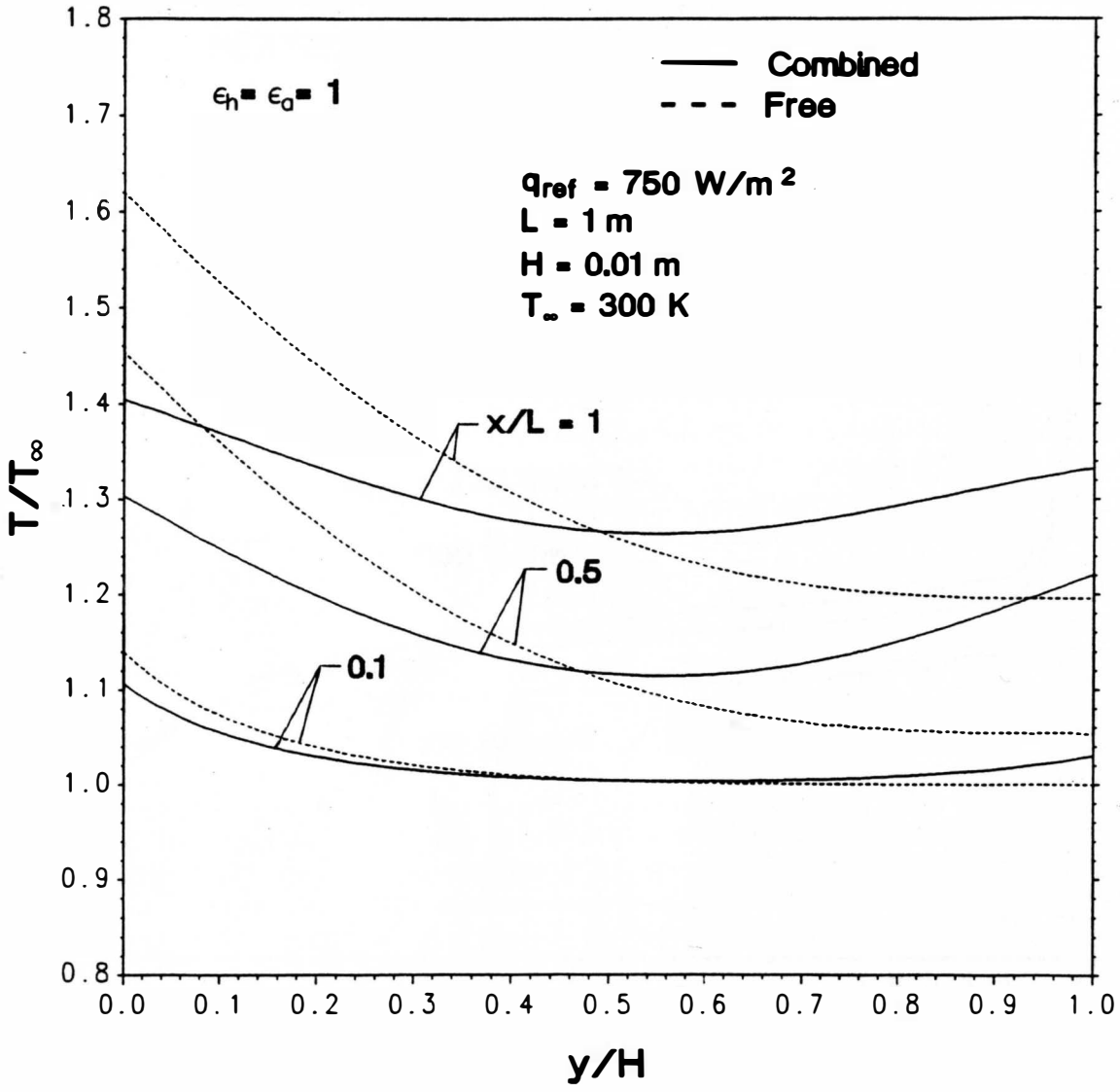

Fig. 4 Transverse temperature profiles air

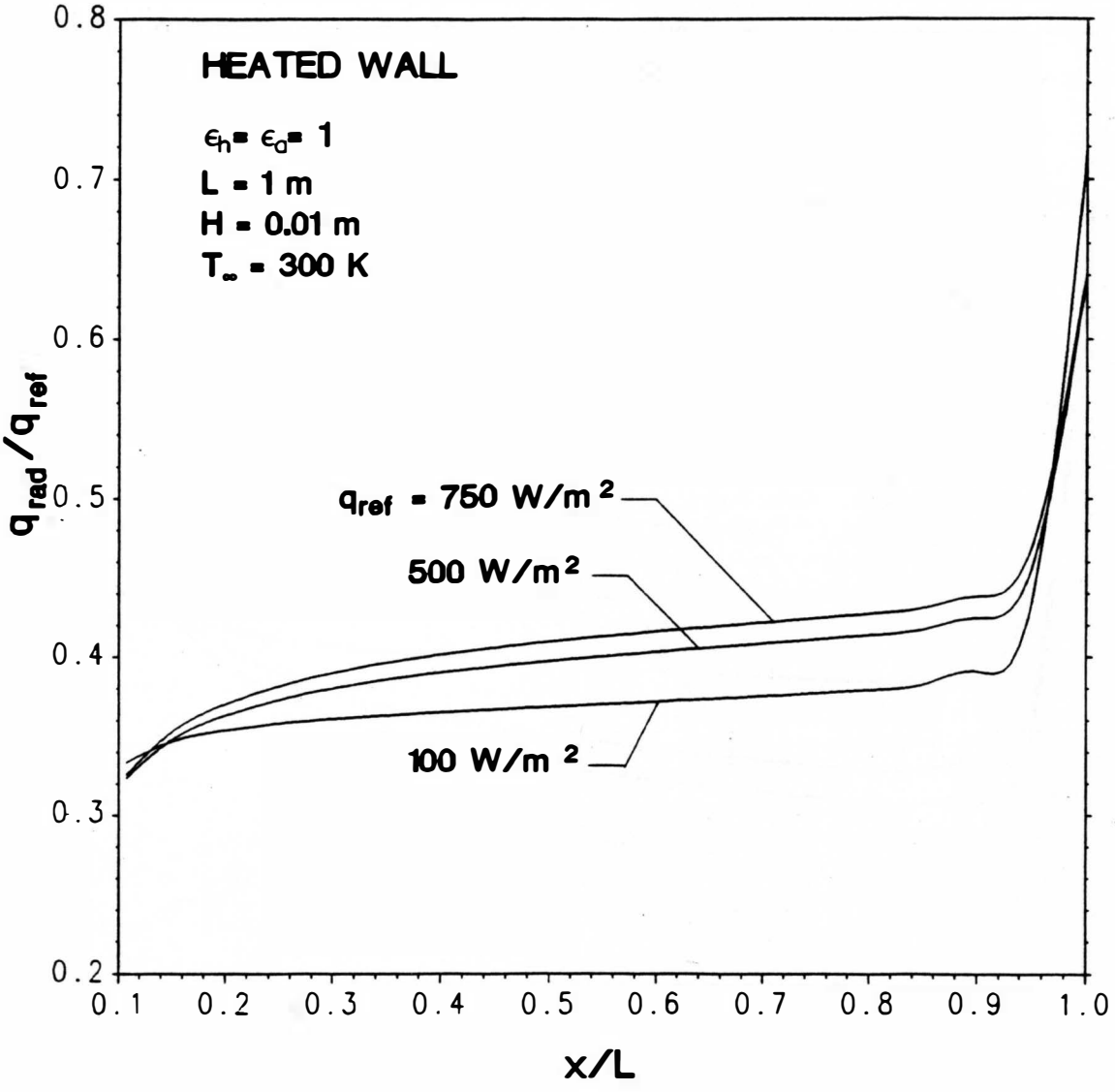

Fig. 5 Fraction of net radiative heat transfer from heated wall.

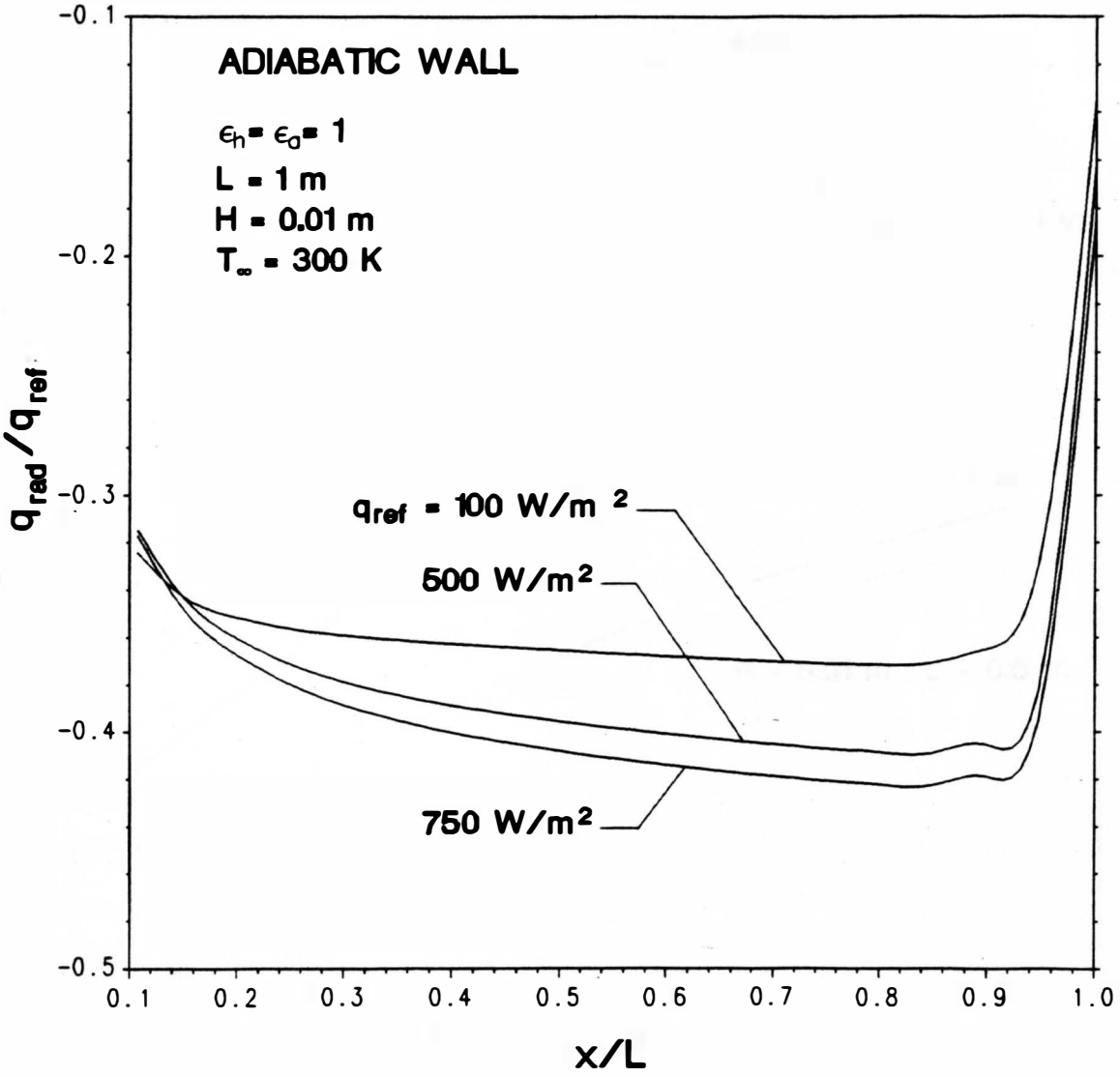

Fig. 6 Fraction of net radiative heat transfer from adiabatic wall.

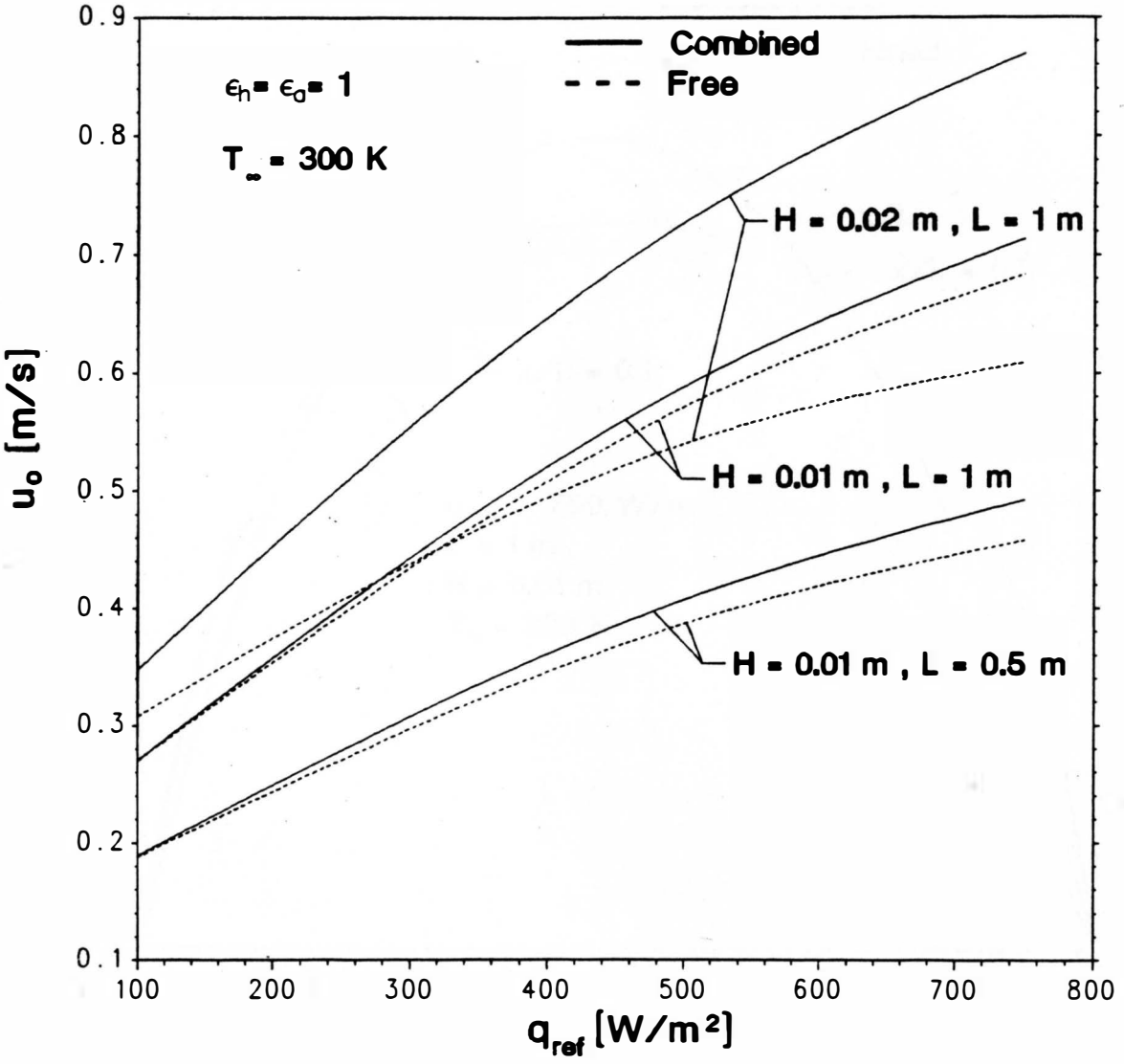

Fig. 7 Effect of rate of heat flux on the average velocity of air.

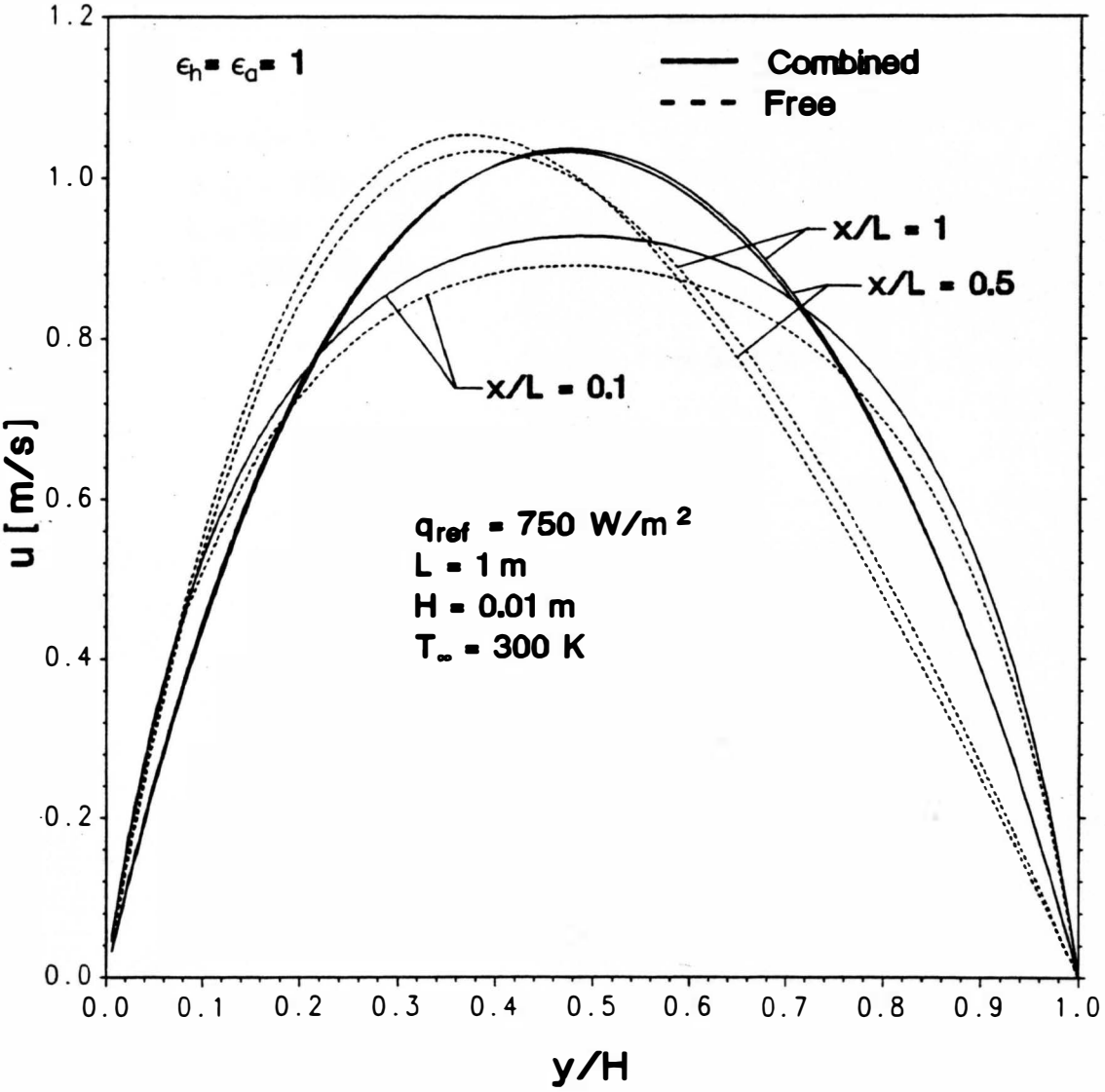

Fig. 8 Transverse velocity profiles of air.

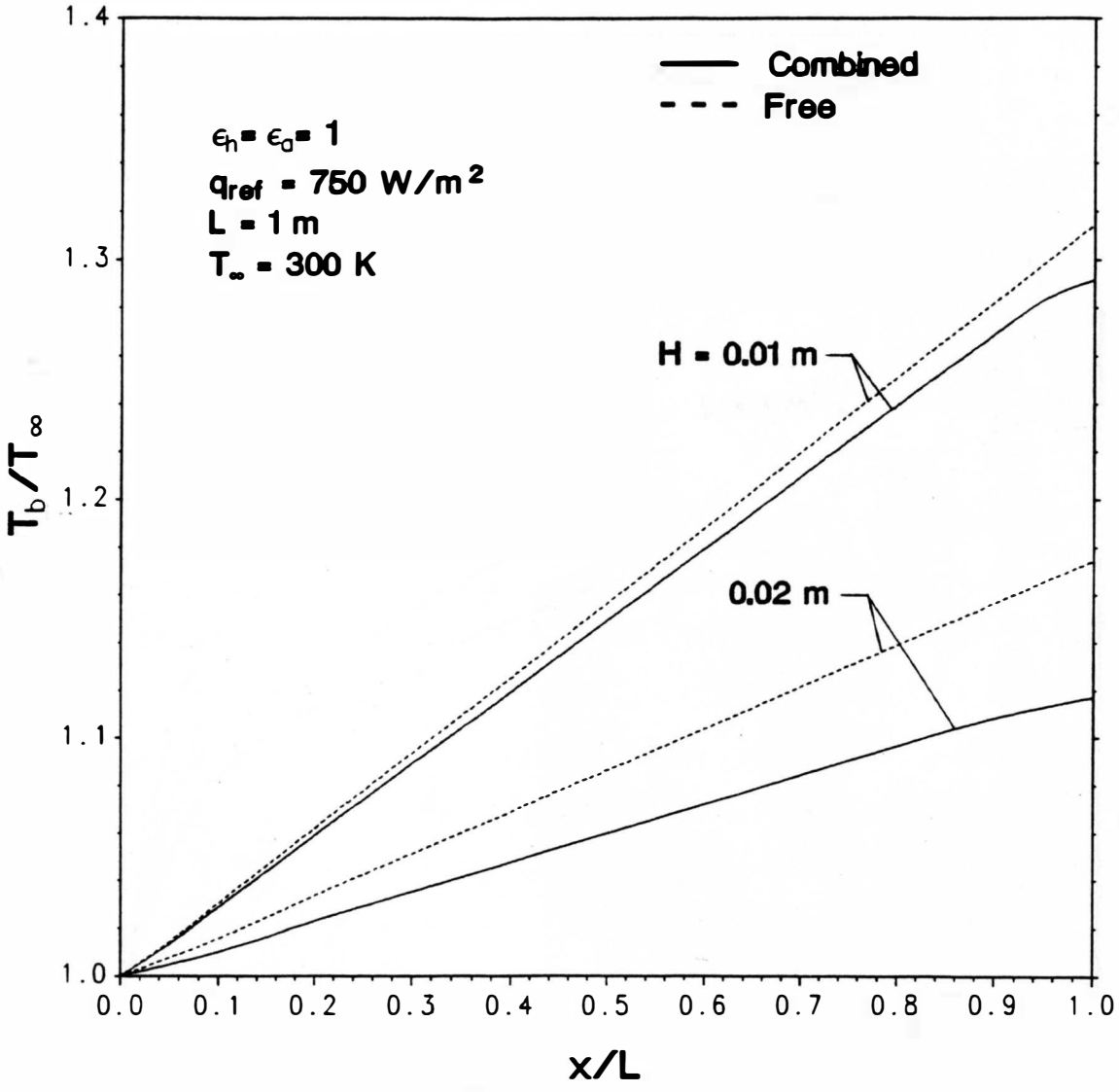

Fig. 9 Axial variation of the bulk temperature of air.

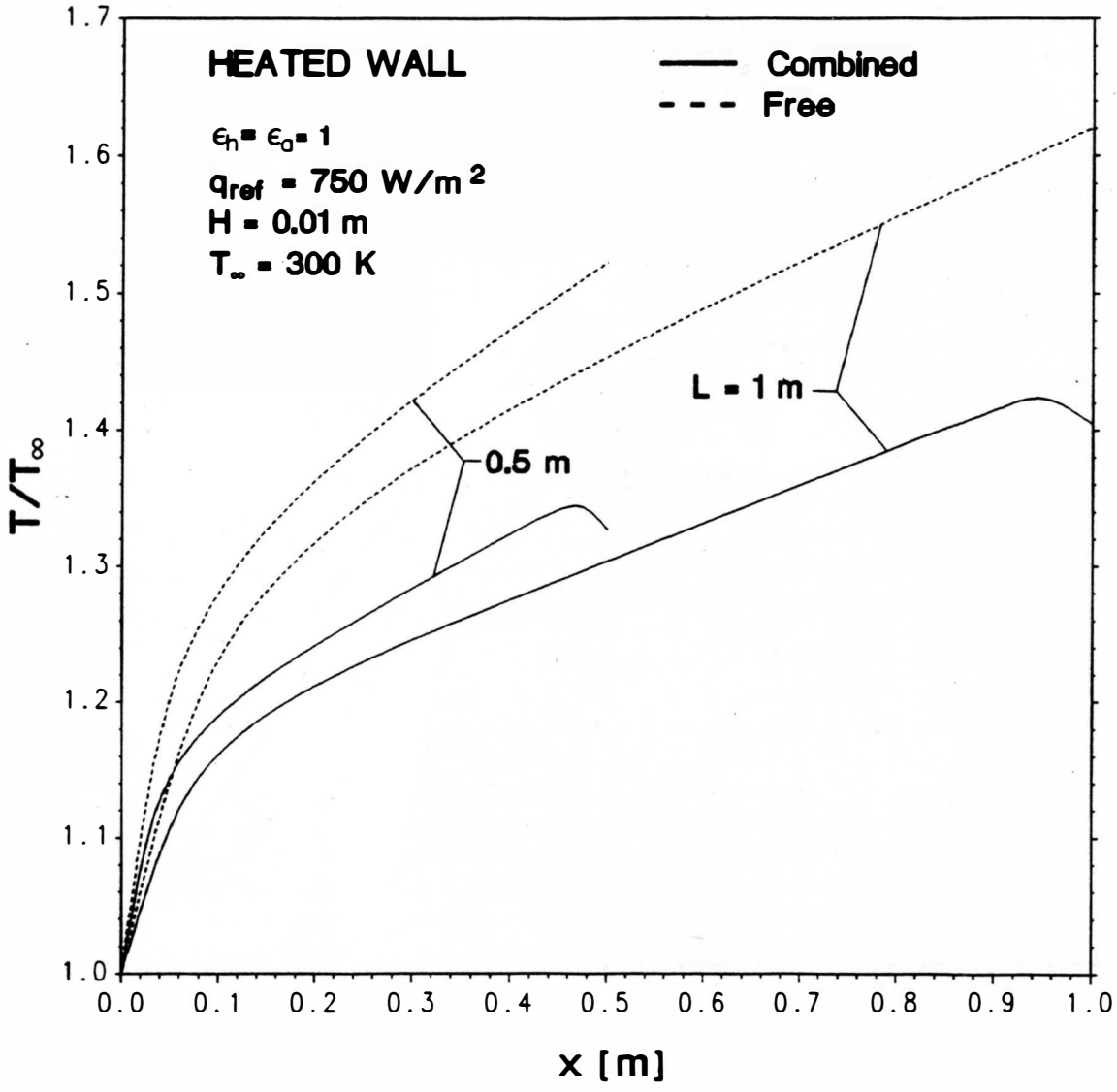

Fig. 10 Effect of channel length on heated wall temperature.

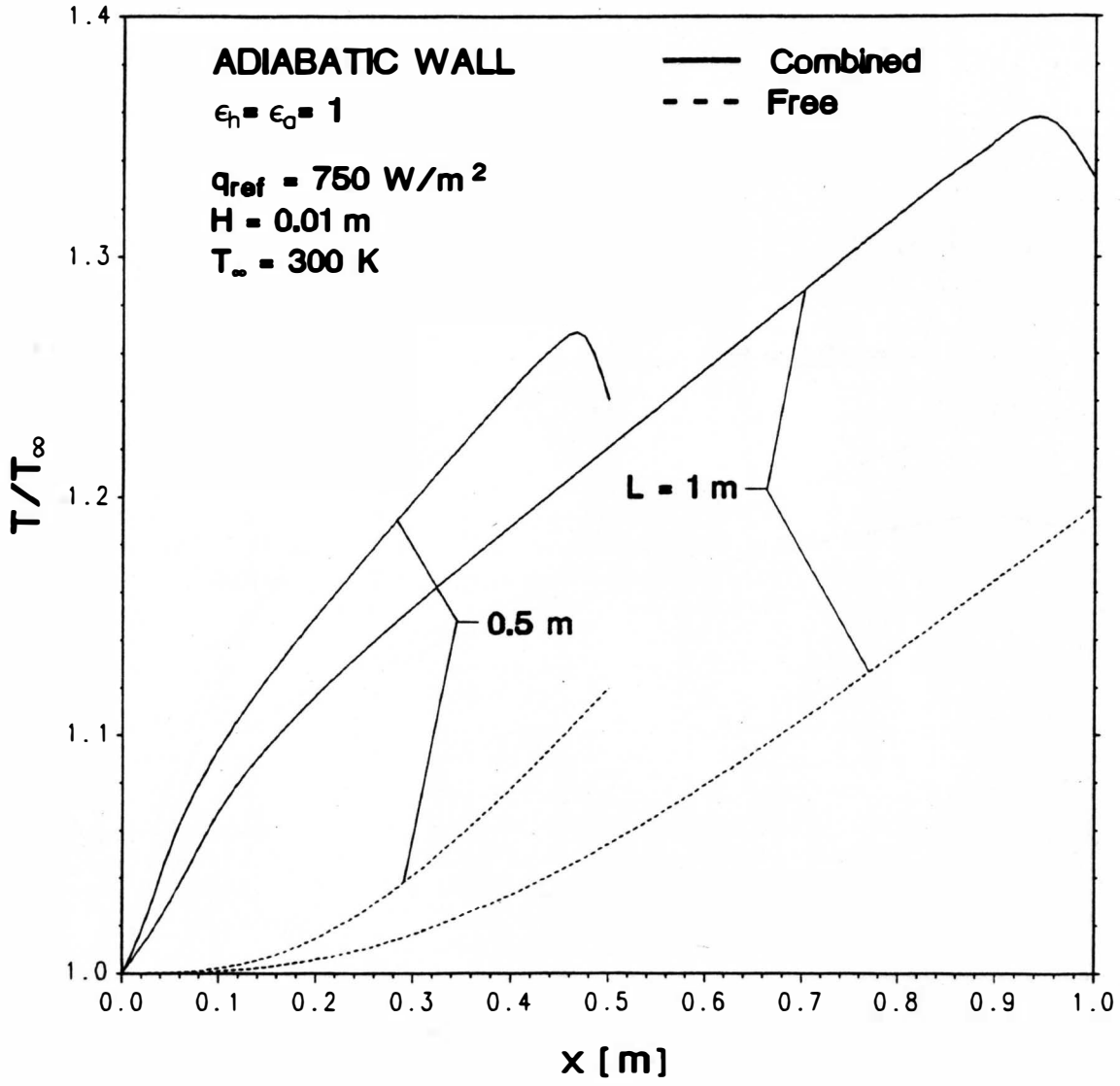

Fig. 11 Effect of channel length on adiabatic wall temperature.

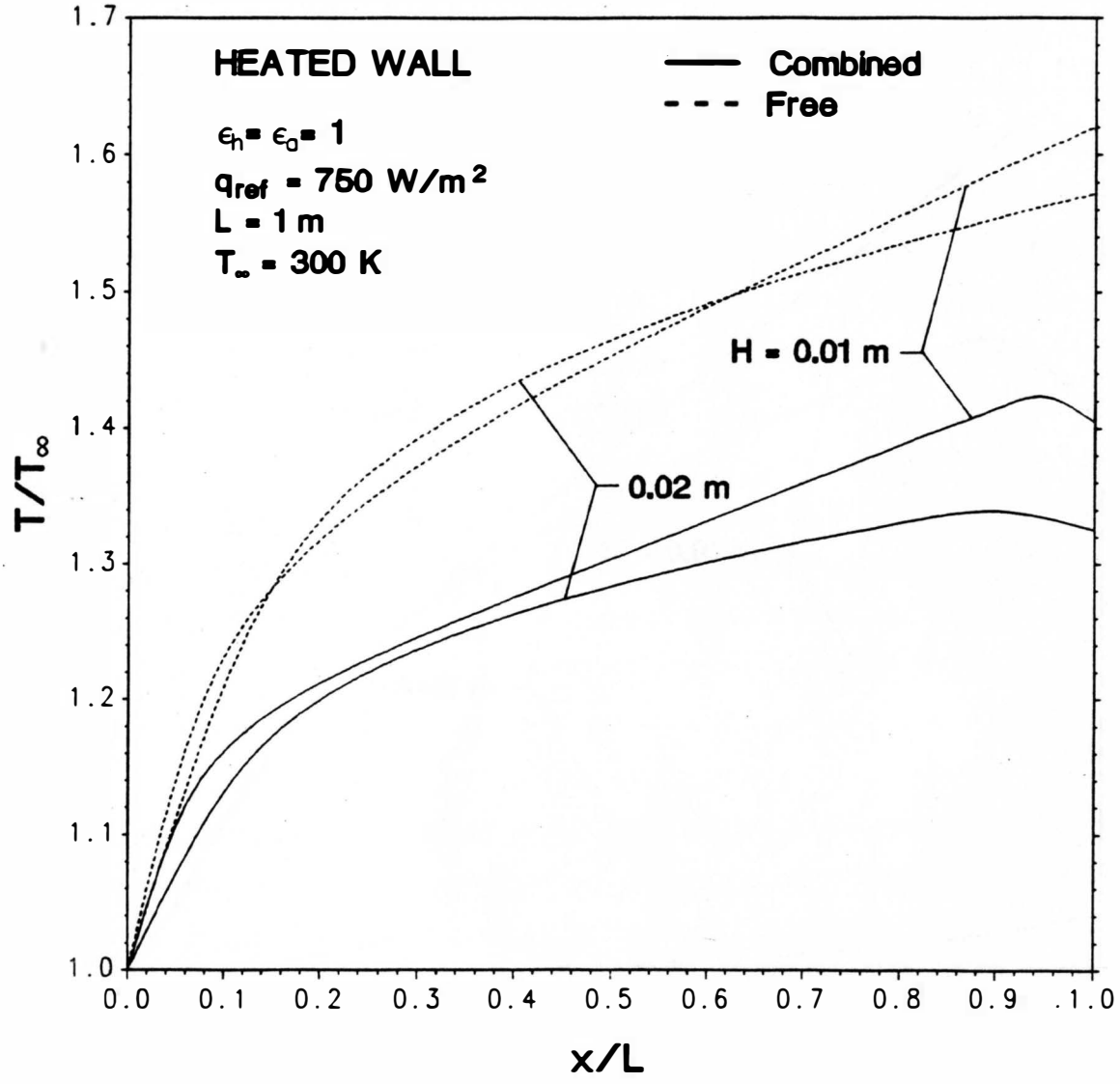

Fig. 12 Effect of channel width on heated wall temperature.

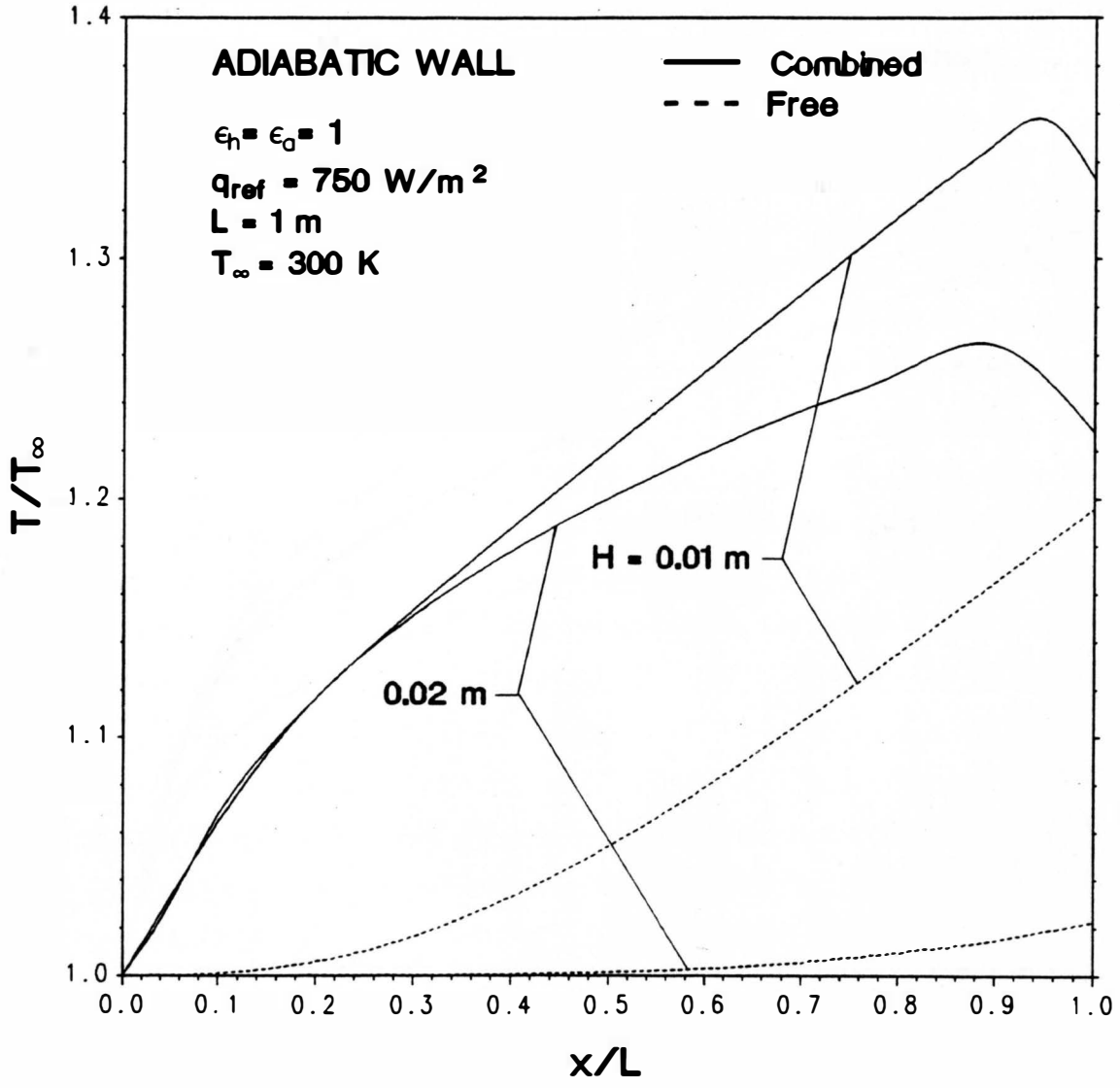

Fig. 13 Effect of channel width on adiabatic wall temperature.

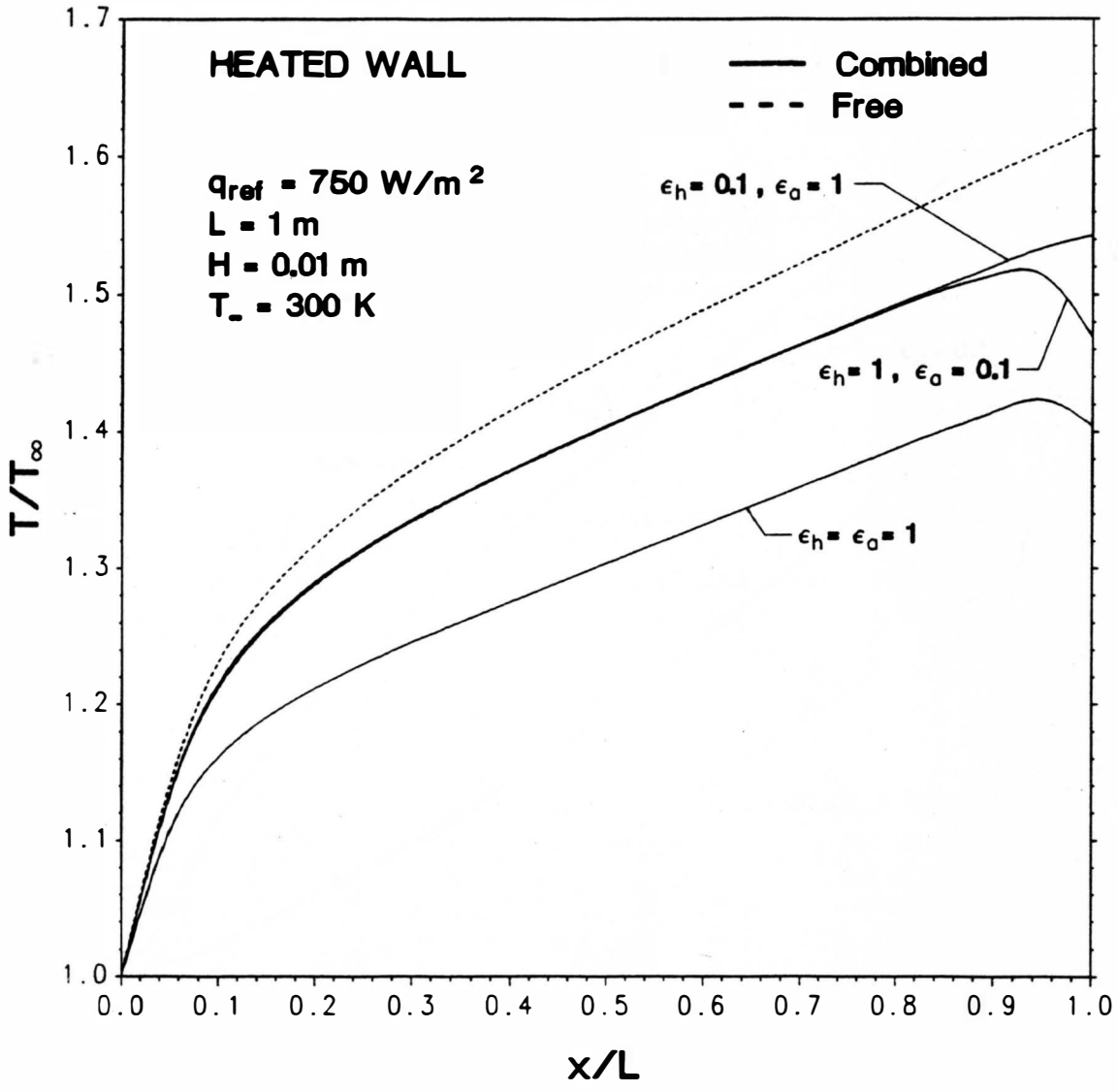

Fig. 14 Effect of surface emissivities on heated wall temperature.

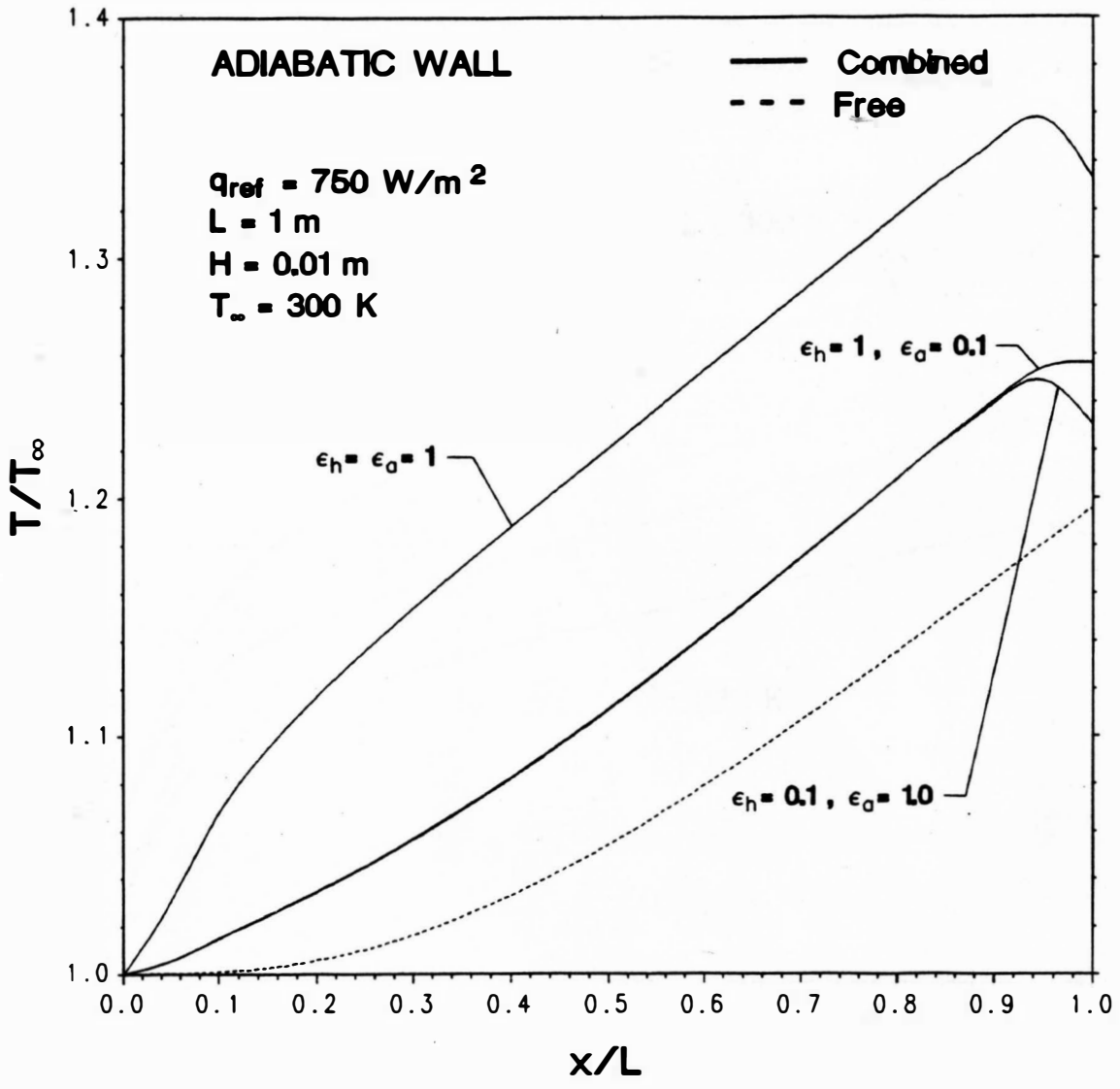

Fig. 15 Effect of surface emissivities on adiabatic wall temperature.

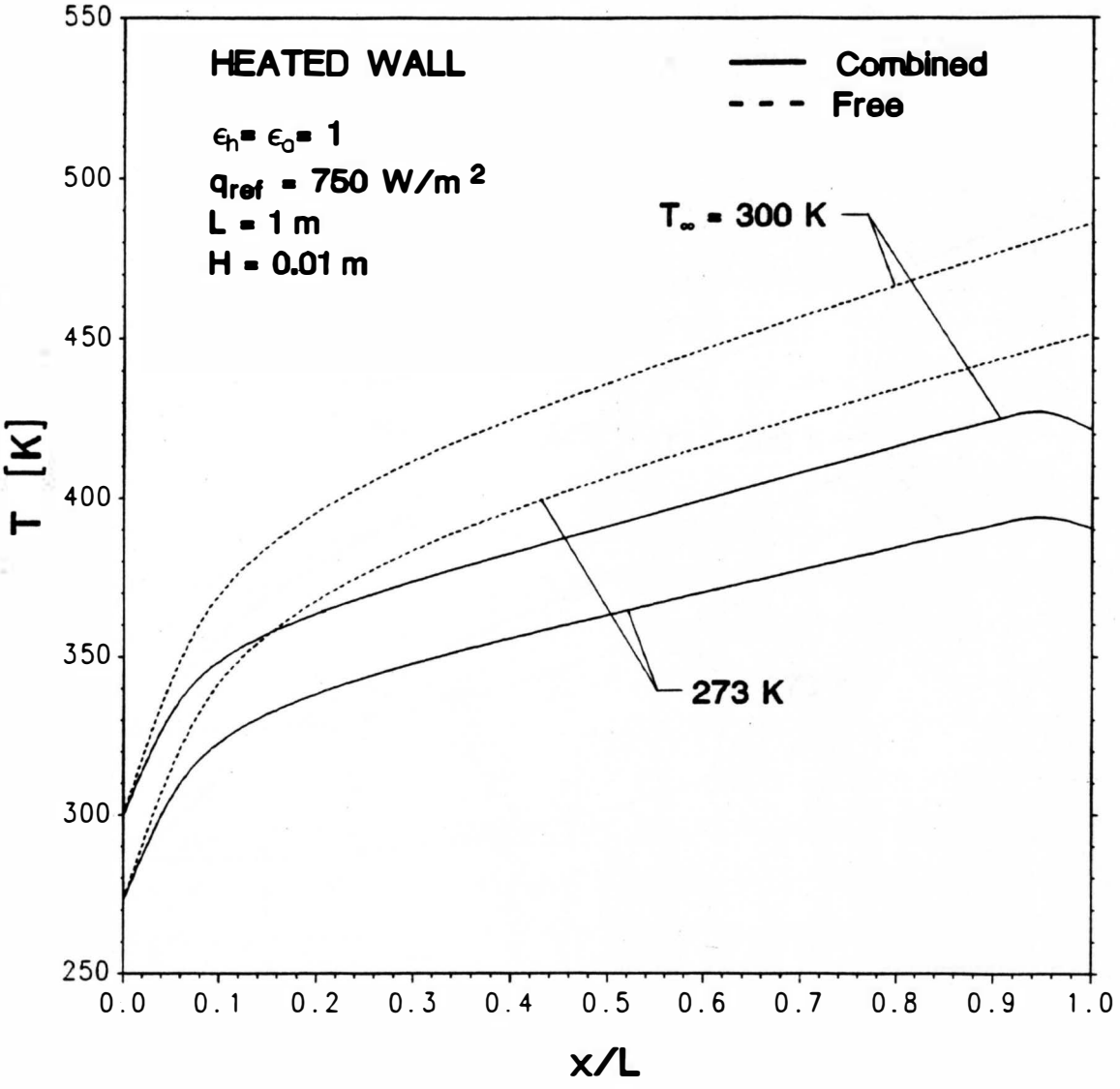

Fig. 16 Effect of inlet air temperature on heated wall temperature.

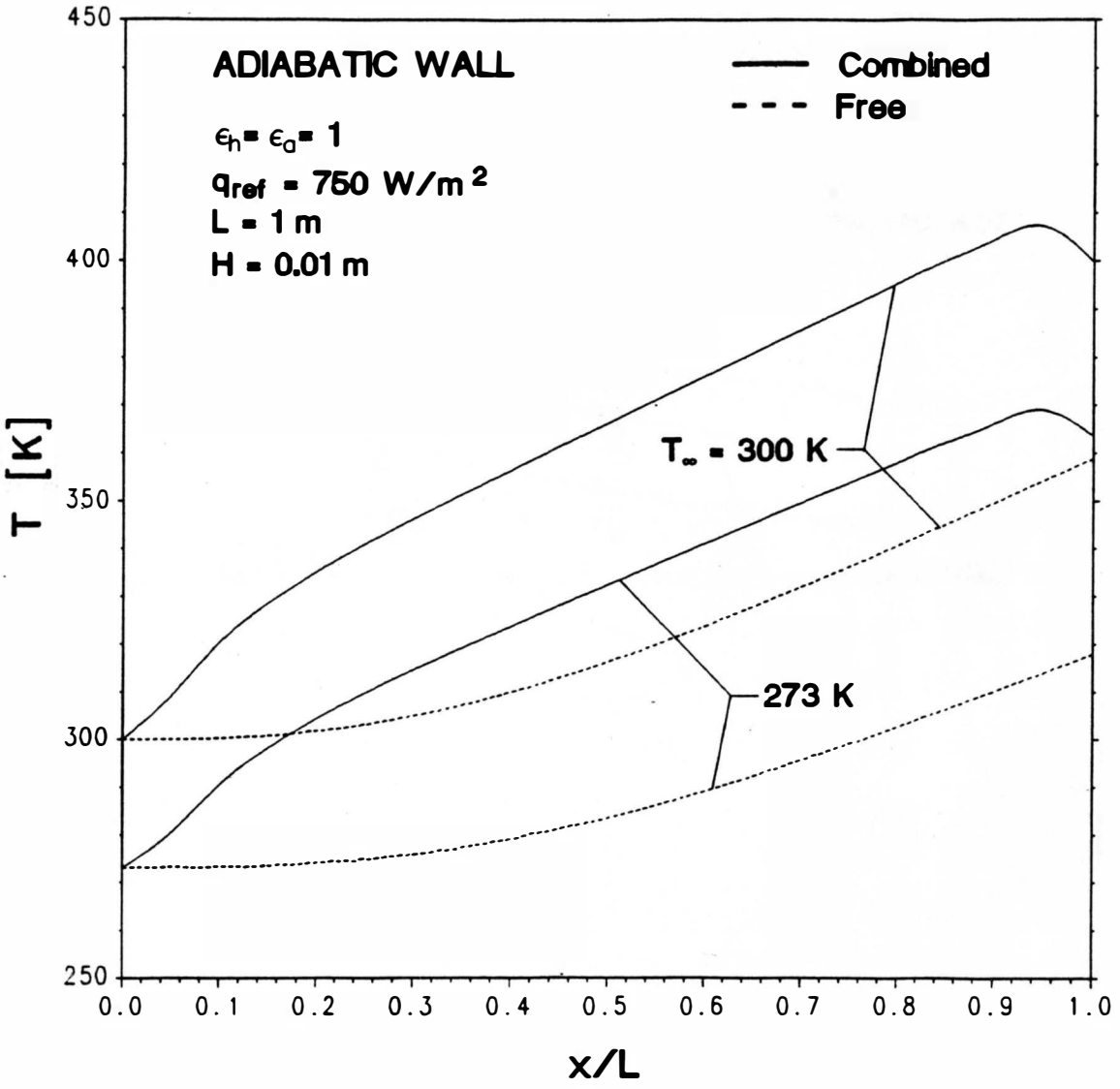

Fig. 17 Effect of inlet air temperature on adiabatic wall temperature.

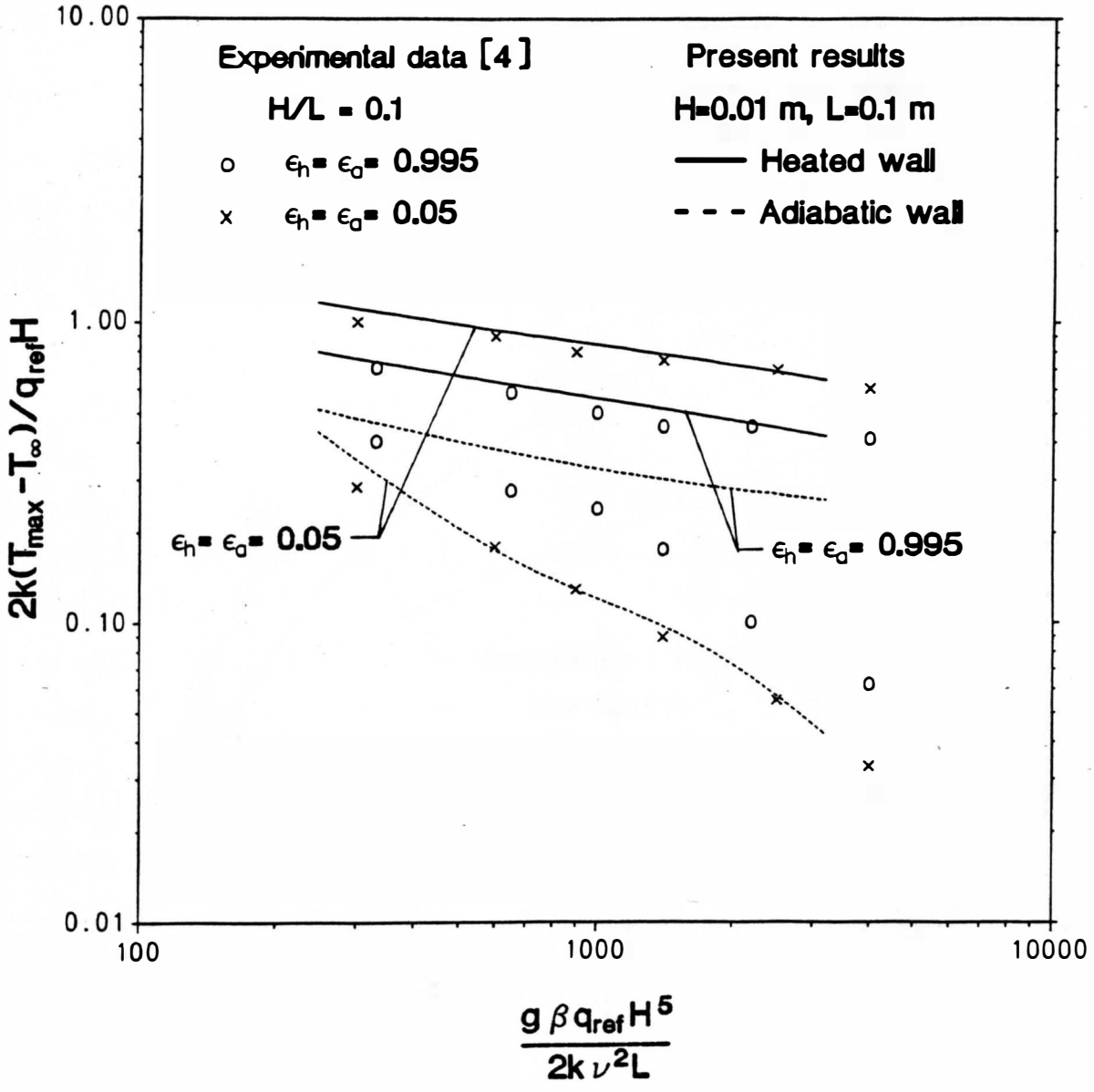

Fig. 18 A comparison of the maximum temperature for the heated and adiabatic walls between experimental and predicted data.

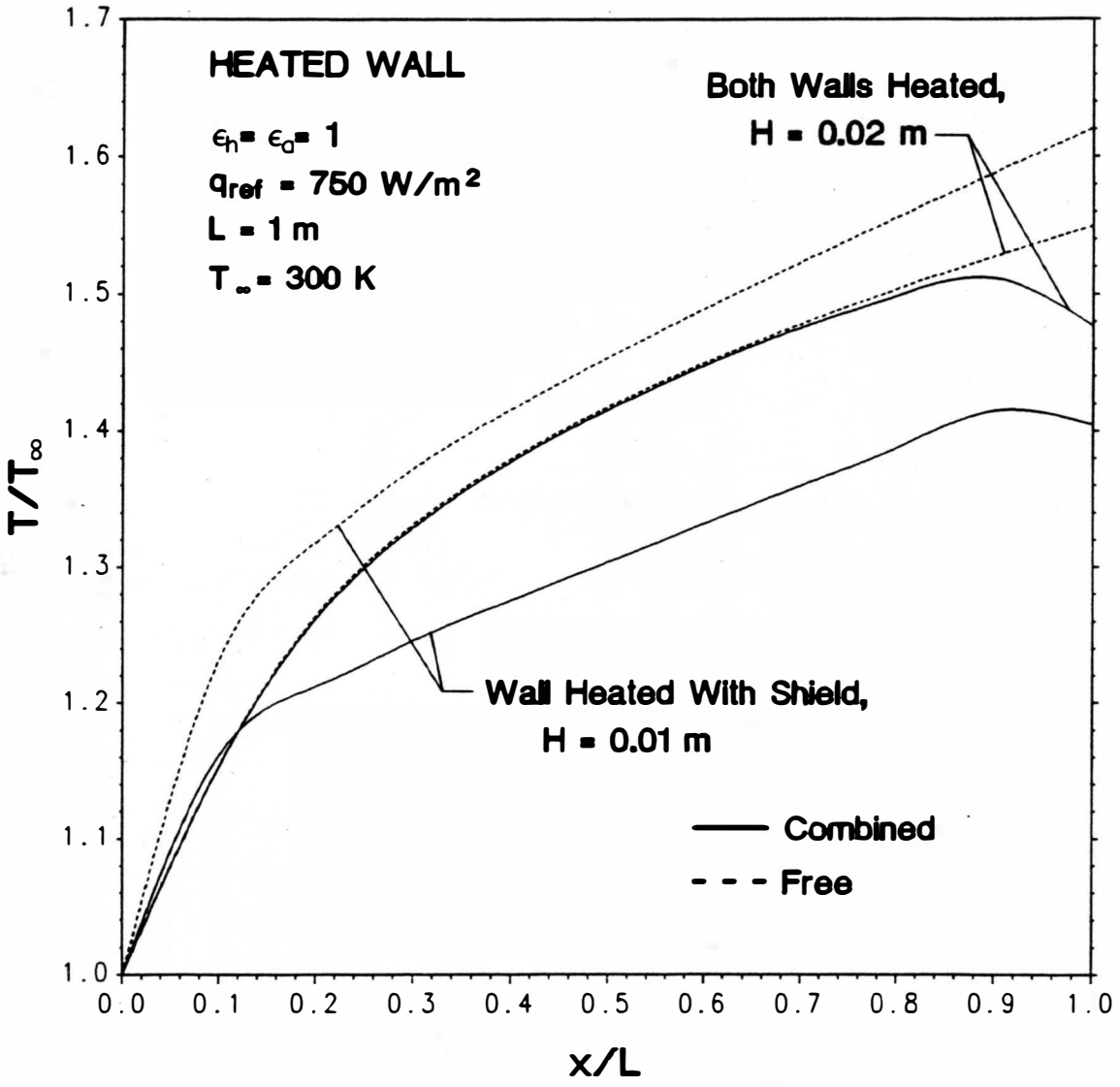

Fig. 19 Effect of placing a shield in the middle of a channel heated uniformly on both walls.

APPENDIX A

Nondimensionalization of the system of differential equations.

APPENDIX A

The material in this appendix is on the transformation of the governing dimensional equations to dimensionless form. The fluid considered is assumed to be incompressible. Thus, the Boussinesq approximation is used to account for the variable density that induces fluid motion.

The following governing equations are to be considered.

$$\frac{\partial u}{\partial x} + \frac{\partial v}{\partial y} = 0 \tag{A.1}$$

$$\rho\left(u\frac{\partial u}{\partial x} + v\frac{\partial u}{\partial y}\right) = -\frac{dp}{dx} + \mu\frac{\partial^2 u}{\partial y^2} - \rho g \tag{A.2}$$

$$\rho\left(u\frac{\partial v}{\partial x} + v\frac{\partial v}{\partial y}\right) = -\frac{dp}{dy} + \mu\frac{\partial^2 v}{\partial y^2} \tag{A.3}$$

$$u\frac{\partial T}{\partial x} + v\frac{\partial T}{\partial y} = \alpha\frac{\partial^2 T}{\partial y^2} \tag{A.4}$$

Let the pressure distribution be expressed by $p'(x,y) = p(x,y) + p_\infty(x)$. By taking the derivative of p', the expression becomes

$$\frac{\partial p}{\partial x} = \frac{\partial p'}{\partial x} + \frac{\partial p_\infty}{\partial x} \tag{A.5}$$

However, outside of the channel where u = v = 0, the second term at the right hand side of equation (A.5) reduces to

$$\frac{\partial p_\infty}{\partial x} = -\rho_\infty g \tag{A.6}$$

or from equation (A.5)

$$\frac{\partial p}{\partial x} = \frac{\partial p'}{\partial x} - \rho_\infty g \tag{A.7}$$

Substituting equation (A.7) into (A.2), we obtain the following equation

$$\rho\left(u\frac{\partial u}{\partial x} + v\frac{\partial u}{\partial y}\right) = -\frac{\partial p'}{\partial x} + \mu\frac{\partial^2 u}{\partial y^2} + (\rho_\infty - \rho) \tag{A.8}$$

According to the Boussinesq approximation:

$$\rho = \rho_\infty + \frac{\partial \rho}{\partial T}(T - T_\infty)$$

where $\partial\rho/\partial T = -\rho\beta$ and β is the expansion coefficient, it follows that

$$(\rho_\infty - \rho) = \rho\beta(T - T_\infty) \tag{A.9}$$

Substituting equation (A.9) into equation (A.8), the x-momentum equation becomes

$$u\frac{\partial u}{\partial x} + v\frac{\partial u}{\partial y} = -\frac{1}{\rho}\frac{\partial p'}{\partial x} + \nu\frac{\partial^2 u}{\partial y^2} + g\beta(T - T_\infty) \tag{A.10}$$

To decouple the longitudinal and lateral pressure gradients, we can represent the local pressure $p'(x,y)$ as the sum of a cross-sectional mean pressure $\bar{p}(x)$, which drives the main flow, and a perturbation about the mean $\hat{p}(x,y)$ which drives the cross-stream flow.

$$p'(x,y) = \bar{p}(x) + \hat{p}(x,y) \tag{A.11}$$

Thus, the set of equations that govern the combined convection and radiation take the form

$$\frac{\partial u}{\partial x} + \frac{\partial v}{\partial y} = 0 \tag{A.12}$$

$$u\frac{\partial u}{\partial x} + v\frac{\partial u}{\partial y} = -\frac{1}{\rho}\frac{\partial \bar{p}}{\partial x} + \nu\frac{\partial^2 u}{\partial y^2} + g\beta(T - T_\infty) \tag{A.13}$$

$$u\frac{\partial v}{\partial x} + v\frac{\partial v}{\partial y} = -\frac{1}{\rho}\frac{\partial \hat{p}}{\partial y} + \nu\frac{\partial^2 v}{\partial y^2} \tag{A.14}$$

$$u\frac{\partial T}{\partial x} + v\frac{\partial T}{\partial y} = \alpha\frac{\partial^2 T}{\partial y^2} \tag{A.15}$$

For the case shown in Fig. (1) where the left wall is uniformly heated while the right wall is adiabatic, equations (A.12-A.15) must be solved subject to boundary conditions of the form

$$
\begin{aligned}
T &= T_{\infty} && \text{at } x = 0 \\
v &= 0 && \text{at } x = 0 \\
\bar{p} &= 0 && \text{at } x = 0 \\
\bar{p} &= 0 && \text{at } x = L \\
u &= v = 0 && \text{at } y = 0 \text{ and } y = H
\end{aligned}
\qquad (A.16)
$$

Let us now consider the dimensionless parameters that govern free convective flow and heat transfer. Introducing

$$X = \frac{x}{HGr_H^*} \qquad U = \frac{uH}{\nu Gr_H^*}$$

$$Y = \frac{y}{H} \qquad V = \frac{vH}{\nu} \qquad (A.17a)$$

$$\bar{P} = \frac{\bar{p}H^2}{\rho\nu^2 Gr_H^{*2}} \qquad P = \frac{pH^2}{\rho\nu^2}$$

$$\theta = \frac{kT}{q_{ref}H}$$

$$Gr_H^* = \frac{g\beta q_{ref}H^4}{\nu^2 k}$$

where Gr_H^* is the modified Grashof Number based on q_{ref}.

The nondimensionalization of the governing equations can be obtained by introducing the following dimensionless parameters.

$$U = \frac{uH}{\nu Gr_H^*} \quad \text{----------} > \quad u = \frac{U\nu Gr_H^*}{H}$$

$$V = \frac{v\,H}{\nu} \quad \text{----------} > \quad v = \frac{V\,\nu}{H}$$

$$X = \frac{x}{HGr_H^*} \quad \text{----------} > \quad x = XHGr_H^*$$

$$Y = \frac{y}{H} \quad \text{----------} > \quad y = YH \qquad \text{(A.17b)}$$

$$\bar{P} = \frac{\bar{p}H^2}{\rho\nu^2 Gr_H^{*2}} \quad \text{----------} > \quad \bar{p} = \frac{\bar{P}\rho\nu^2 Gr_H^{*2}}{H^2}$$

$$\theta = \frac{kT}{q_{ref}H} \quad \text{----------} > \quad T = \frac{q_{ref}H\theta}{k}$$

$$\hat{P} = \frac{\hat{p}H^2}{\rho\nu^2} \quad \text{----------} > \quad \hat{p} = \frac{\hat{P}\rho\nu^2}{H^2}$$

The nondimensionalization of the continuity equation is shown as follows:

$$\frac{\partial u}{\partial x} + \frac{\partial v}{\partial y} = 0 \qquad (A.18)$$

By introducing the dimensionless parameters (equation A.17) to equation (A.18), gives

$$\frac{\partial(U\nu Gr^{*}/H)}{\partial(XHGr^{*})} + \frac{\partial(V\nu/H)}{\partial(YH)} = 0 \qquad (A.19)$$

Since ν, Gr and H are constant quantities, equation (A.19) is written as

$$\frac{\partial U}{\partial X} + \frac{\partial V}{\partial Y} = 0 \qquad (A.20)$$

A similar approach is used to nondimensionalize the x-momentum equation

$$u\frac{\partial u}{\partial x} + v\frac{\partial u}{\partial y} = -\frac{1}{\rho}\frac{\partial \bar{p}}{\partial x} + \nu\frac{\partial^2 u}{\partial y^2} + g\beta(T - T_{\infty}) \qquad (A.21)$$

The following equations are obtained by substituting the dimensionless parameters of equation (B.17) into (A.21) which gives:

$$\frac{U\nu Gr^*}{H}\frac{\partial(U\nu Gr^*/H)}{\partial(XHGr^*)} + \frac{V\nu}{H}\frac{\partial(U\nu Gr^*/H)}{\partial(YH)} = -\frac{1}{\rho}\frac{\partial(\bar{P}\rho\nu^2Gr^{*2}/H)}{\partial(XHGr^*)}$$

$$+ \nu\frac{\partial^2(U\nu Gr^*/H)}{\partial(YH)^2} + g\beta\frac{q_{ref}H}{k}(\theta - \theta_\infty)$$

$$\frac{U\nu Gr^*/H}{H^3Gr^*}\frac{\partial U}{\partial X} + \frac{V\nu^2Gr^*}{H^3}\frac{\partial U}{\partial Y} = -\frac{1}{\rho}\frac{\rho\nu^2Gr^{*2}}{H^3Gr^*}\frac{\partial\bar{P}}{\partial X} + \frac{\nu^2Gr^*}{H^3}\frac{\partial^2U}{\partial Y^2}$$

$$+ g\beta\frac{q_{ref}H}{k}(\theta - \theta_\infty)$$

$$U\frac{\partial U}{\partial X} + V\frac{\partial U}{\partial Y} = -\frac{\partial\bar{P}}{\partial X} + \frac{\partial^2U}{\partial Y^2} + \frac{g\beta q_{ref}H}{k}\frac{H^3}{\nu^2Gr^*}(\theta - \theta_\infty)$$

$$U\frac{\partial U}{\partial X} + V\frac{\partial U}{\partial Y} = -\frac{\partial\bar{P}}{\partial X} + \frac{\partial^2U}{\partial Y^2} + (\theta - \theta_\infty) \qquad \text{(A.22)}$$

Similarly, the nondimensionalization of the y-momentum equation is obtained as follows:

$$u\frac{\partial v}{\partial x} + v\frac{\partial v}{\partial y} = -\frac{1}{\rho}\frac{\partial\hat{p}}{\partial y} + \nu\frac{\partial^2v}{\partial y^2} \qquad \text{(A.23)}$$

$$\frac{U\nu Gr^*}{H}\frac{\partial(V\nu/H)}{\partial(XHGr^*)} + \frac{V\nu}{H}\frac{\partial(V\nu/H)}{\partial(YH)} = -\frac{1}{\rho}\frac{\partial(\hat{P}\rho\nu^2/H^2)}{\partial(YH)} + \nu\frac{\partial^2(V\nu/H)}{\partial(YH)^2}$$

$$\frac{\nu^2}{H^3}U\frac{\partial V}{\partial X} + \frac{\nu^2}{H^3}V\frac{\partial V}{\partial Y} = -\frac{\nu^2}{H^3}\frac{\partial \hat{P}}{\partial Y} + \frac{\nu^2}{H^3}\frac{\partial^2 V}{\partial Y^2}$$

$$U\frac{\partial V}{\partial X} + V\frac{\partial V}{\partial Y} = -\frac{\partial \hat{P}}{\partial Y} + \frac{\partial^2 V}{\partial Y^2} \qquad (A.24)$$

Lastly, the energy equation can be nondimensionalized as shown below

$$u\frac{\partial T}{\partial x} + v\frac{\partial T}{\partial y} = \alpha\frac{\partial^2 T}{\partial y^2} \qquad (A.25)$$

$$\frac{U\nu Gr^*}{H}\frac{\partial(q_{ref}H\theta/K)}{\partial(XHGr^*)} + \frac{V\nu}{H}\frac{\partial(q_{ref}H\theta/K)}{\partial(YH)} = \alpha\frac{\partial^2(q_{ref}H\theta/K)}{\partial(YH)^2}$$

$$\frac{\nu}{H^2}U\frac{\partial \theta}{\partial X} + \frac{\nu}{H^2}V\frac{\partial \theta}{\partial Y} = \frac{\alpha}{H^2}\frac{\partial^2 \theta}{\partial Y^2}$$

$$U\frac{\partial \theta}{\partial X} + V\frac{\partial \theta}{\partial Y} = \frac{1}{Pr}\frac{\partial^2 \theta}{\partial Y^2} \qquad (A.26)$$

The set of dimensionless equations that govern the combined free convection and radiation are thus summarized as:

$$\frac{\partial U}{\partial X} + \frac{\partial V}{\partial Y} = 0 \tag{A.27}$$

$$U\frac{\partial U}{\partial X} + V\frac{\partial U}{\partial Y} = -\frac{\partial \bar{P}}{\partial X} + \frac{\partial^2 U}{\partial Y^2} + (\theta - \theta_\infty) \tag{A.28}$$

$$U\frac{\partial V}{\partial X} + V\frac{\partial V}{\partial Y} = -\frac{\partial \hat{P}}{\partial Y} + \frac{\partial^2 V}{\partial Y^2} \tag{A.29}$$

$$U\frac{\partial \theta}{\partial X} + V\frac{\partial \theta}{\partial Y} = \frac{1}{Pr}\frac{\partial^2 \theta}{\partial Y^2} \tag{A.30}$$

APPENDIX B

Derivation of the thermal boundary conditions.

APPENDIX B

This appendix is on the derivation of the thermal boundary conditions.

Thermal Boundary condition

The thermal boundary condition on the left surface can be derived by employing the energy balance. It can be written as:

$$q_i = q_{ic} + q_{ir} \tag{B.1}$$

where the subscript i, is for an element at the left surface, while the subscripts c and r denote convection and radiation respectively. The convection term in Equation (B.1) is given by Fourier's law $-k(\partial T_i/\partial y)_i$, whereas the radiation term can be written as:

$$q_{ir} = \varepsilon_i \sigma T_i^4 - \alpha_i G_i \tag{B.2}$$

whereby ε_i, σ, T_i and α_i are emissivity, Stefan-Boltzmann constant, surface temperature and absorptivity respectively. The first term on the right hand side of equation (B.2) is the radiative flux emitted by the surface whereas the second term is net radiative flux absorbed by the element at the left surface. G denotes irradiation. Rearranging equation (B.2) for an opaque surface gives:

(B.5), for opaque surfaces, one will arrive at the equation shown below:

$$q_m = k\frac{\partial T_m}{\partial y}\bigg|_{y=H} + \varepsilon_m \sigma T_m^4 - \varepsilon_m \left[- q_m + k\frac{\partial T_m}{\partial y}\bigg|_{y=H} + J_m \right] \qquad (B.7)$$

$$m = 1, 2, 3, \ldots, N.$$

Solving equation (B.7) for J_m gives

$$J_m = \frac{(1-\varepsilon_m)}{\varepsilon_m} \left[\frac{\partial T_m}{\partial y}\bigg|_{y=H} - q_m \right] + \sigma T_m^4 \qquad (B.8)$$

$$m = 1, 2, 3, \ldots, N.$$

Substituting equation (B.8) into (B.4), the following equation can be written:

$$q_i = - k\frac{\partial T_i}{\partial y}\bigg|_{y=0} + \varepsilon_i \sigma T_i^4 - \varepsilon_i \sum_{m=1}^{N} F_{i-m} \left[\frac{(1-\varepsilon_m)}{\varepsilon_m} \left(k\frac{\partial T_m}{\partial y}\bigg|_{y=H} - q_m \right) + \sigma T_m^4 \right] \qquad (B.9)$$

$$m = 1, 2, 3, \ldots, N.$$

When radiative losses to the entrance and exit are taken into consideration, Equation (B.9) becomes

$$q_i = - k\frac{\partial T_i}{\partial y}\bigg|_{y=0} + \varepsilon_i \sigma T_i^4 - \varepsilon_i \sum_{m=1}^{N} F_{i-m}\left[\frac{(1-\varepsilon_m)}{\varepsilon_m}\left(k\frac{\partial T_m}{\partial y}\bigg|_{y=H} - q_m\right) + \sigma T_m^4\right] - \varepsilon_i F_{i\text{-top}}\sigma T_\infty^4 - \varepsilon_i F_{i\text{-bot}}\sigma T_\infty^4 \qquad \text{(B.10)}$$

$$\text{at } i = 1, 2, \ldots, N$$

Similarly, for the right wall,

$$q_j = - k\frac{\partial T_j}{\partial y}\bigg|_{y=H} + \varepsilon_j \sigma T_j^4 - \varepsilon_j \sum_{n=1}^{N} F_{j-n}\left[\frac{(1-\varepsilon_n)}{\varepsilon_n}\left(k\frac{\partial T_n}{\partial y}\bigg|_{y=0} - q_n\right) + \sigma T_n^4\right] - \varepsilon_j F_{j\text{-top}}\sigma T_\infty^4 - \varepsilon_j F_{j\text{-bot}}\sigma T_\infty^4 \qquad \text{(B.11)}$$

$$\text{at } j = 1, 2, \ldots, N$$

The dimensional equation (B.10) and (B.11) have to be nondimensionalized by using the dimensionless parameters given by equation (A.17b).

In nondimensionalizing equation (B.10), one has:

$$q_i = - k\frac{\partial(q_{ref}H\theta_i/k)}{\partial(YH)}\bigg|_{Y=0} + \varepsilon_i\sigma\left(\frac{q_{ref}H\theta_i}{k}\right)^4 - \varepsilon_i \sum_{m=1}^{N} F_{i-m}$$

$$X\left[\frac{(1-\varepsilon_m)}{\varepsilon_m}\left(k\frac{\partial(q_{ref}H\theta_m/k)}{\partial(YH)}\bigg|_{Y=1} - q_m\right) + \sigma\left(\frac{q_{ref}H\theta_m}{k}\right)^4\right]$$

$$- \varepsilon_i F_{i-top}\sigma\left(\frac{q_{ref}H\theta_\infty}{k}\right)^4 - \varepsilon_i F_{i-bot}\sigma\left(\frac{q_{ref}H\theta_\infty}{k}\right)^4 \qquad \text{(B.12)}$$

Rearranging equation (B.12), gives:

$$\frac{q_i}{qref} = - \frac{\partial\theta_i}{\partial Y}\bigg|_{Y=0} + \varepsilon_i\left(\frac{\sigma q_{ref}{}^3H^4}{k^4}\right)\theta_i{}^4 - \varepsilon_i \sum_{m=1}^{N} F_{i-m}$$

$$X\left[\frac{(1-\varepsilon_m)}{\varepsilon_m}\left(\frac{\partial\theta_m}{\partial Y}\bigg|_{Y=1} - \frac{q_m}{q_{ref}}\right) + \left(\frac{\sigma q_{ref}{}^3H^4}{k^4}\right)\theta_m{}^4\right]$$

$$- \varepsilon_i F_{i-top}\left(\frac{\sigma q_{ref}{}^3H^4}{k^4}\right)\theta_\infty{}^4 - \varepsilon_i F_{i-bot}\left(\frac{\sigma q_{ref}{}^3H^4}{k^4}\right)\theta_\infty{}^4 \qquad \text{(B.13)}$$

Introducing a new symbol R, the Radiation number, where R is defined as $(\sigma q_{ref}^3 H^4/k^4)$, equation (B.13) becomes:

$$\frac{q_i}{q_{ref}} = -\left.\frac{\partial\theta_i}{\partial Y}\right|_{Y=0} + \varepsilon_i R\theta_i^4 - \varepsilon_i \sum_{m=1}^{N} F_{i-m}\left[\frac{(1-\varepsilon_m)}{\varepsilon_m}\right.$$

$$\left. X \left(\left.\frac{\partial\theta_m}{\partial Y}\right|_{Y=1} - \frac{q_m}{q_{ref}}\right) + R\theta_m^4\right] - \varepsilon_i F_{i\text{-top}} R\theta_\infty^4$$

$$- \varepsilon_i F_{i\text{-bot}} R\theta_\infty^4 \qquad \text{(B.14)}$$

Similarly, the dimensionless form of equation (B.11) is written as

$$\frac{q_j}{q_{ref}} = -\left.\frac{\partial\theta_j}{\partial Y}\right|_{Y=1} + \varepsilon_j R\theta_j^4 - \varepsilon_j \sum_{n=1}^{N} F_{j-n}\left[\frac{(1-\varepsilon_n)}{\varepsilon_n}\right.$$

$$\left. X \left(\left.\frac{\partial\theta_n}{\partial Y}\right|_{Y=0} - \frac{q_n}{q_{ref}}\right) + R\theta_n^4\right] - \varepsilon_j F_{j\text{-top}} R\theta_\infty^4$$

$$- \varepsilon_j F_{j\text{-bot}} R\theta_\infty^4 \qquad \text{(B.15)}$$

APPENDIX C

Finite difference analysis.

APPENDIX C

FINITE DIFFERENCE SCHEME

The finite-difference scheme introduced by Patankar and Spalding is used to solve the simultaneous differential equations. The governing equations are written with reference to the cartesian co-ordinates x and y:

$$\frac{\partial U}{\partial X} + \frac{\partial V}{\partial Y} = 0$$

$$U\frac{\partial U}{\partial X} + V\frac{\partial U}{\partial Y} = -\frac{\partial P}{\partial X} + \frac{\partial^2 U}{\partial Y^2} + (\theta - \theta_\infty)$$

$$U\frac{\partial V}{\partial X} + V\frac{\partial V}{\partial Y} = -\frac{\partial P}{\partial Y} + \frac{\partial^2 V}{\partial Y^2}$$

$$U\frac{\partial \theta}{\partial X} + V\frac{\partial \theta}{\partial Y} = \frac{1}{Pr}\frac{\partial^2 \theta}{\partial Y^2}$$

It should be noted that the symbol $\bar{P}$ used for the pressure in the x-momentum equation is different from the symbol $\hat{P}$ in the y-momentum equation. The pressure $\bar{P}$ is the averaged pressure over a cross-section whereas $\hat{P}$ is the pressure perturbation.

The task of this section is to employ the finite difference method to the governing equations, in obtaining a solution for ϕ in the presence of a given flow field (the velocity components).

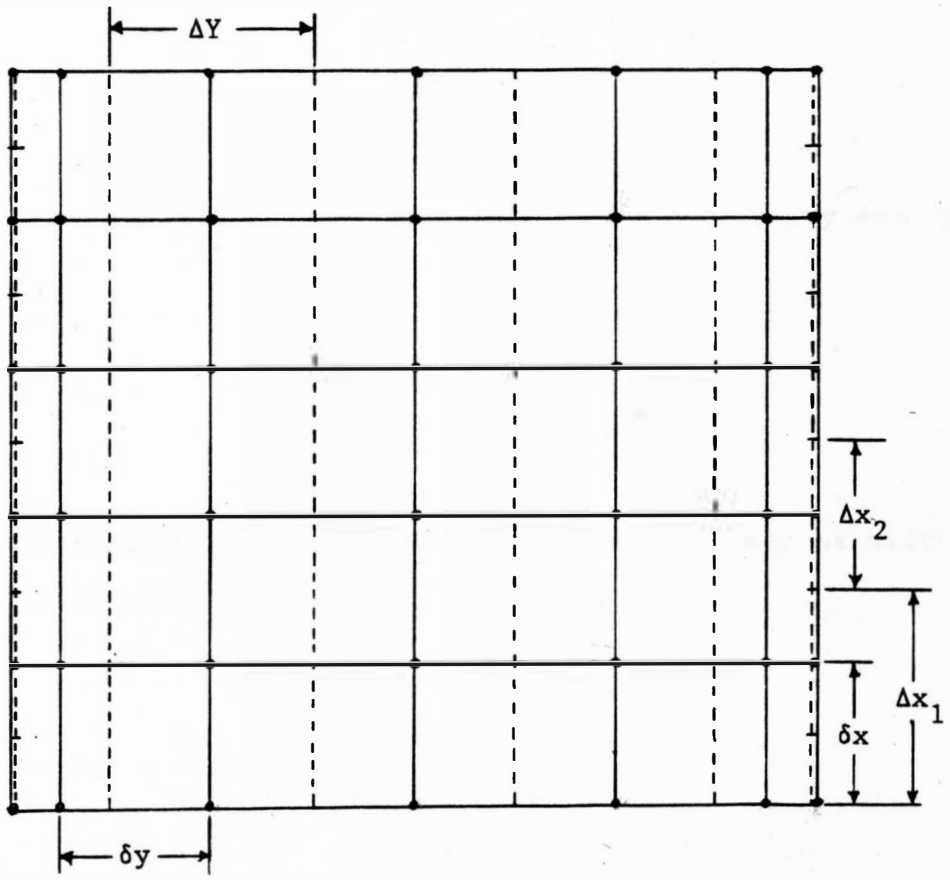

Fig. (C.1) Control volume for the channel flow.

Finite difference method for the x-Momentum Equation.

It should be noted that the convection term has an inseparable connection with the diffusion term, and therefore, the two terms need to be handled as one unit. From Appendix A, the x-momentum equation is written as

$$U\frac{\partial U}{\partial X} + V\frac{\partial U}{\partial Y} = -\frac{\partial \bar{P}}{\partial X} + \frac{\partial^2 U}{\partial Y^2} + (\theta - \theta_\infty) \qquad (C.1)$$

Since the flow field must satisfy the continuity equation

$$U\frac{\partial U}{\partial X} + V\frac{\partial U}{\partial Y} = 0 \qquad (C.2)$$

the general differential equation of the x-momentum may be written in term of ϕ as

$$\frac{\partial}{\partial X}(\rho U\phi) + \frac{\partial}{\partial Y}(\rho V\phi) - \frac{\partial}{\partial Y}\left(\frac{\partial \phi}{\partial Y}\right) = -\frac{\partial \bar{P}}{\partial X} + (\theta - \theta_\infty) \qquad (C.3)$$

Where in this case ϕ is the dimensionless x-component velocity, U. Equation (C.3) can also be written as

$$\frac{\partial J_x}{\partial X} + \frac{\partial J_y}{\partial Y} = - \frac{\partial \bar{P}}{\partial X} + (\theta - \theta_\infty) \qquad (C.4)$$

where J is the total flux and is made up of the convection flux $\rho U\phi$ and the diffusion flux $-\Gamma(\partial\phi/\partial Y)$. Since the flow is considered as parabolic flow, the J's are defined as

$$J_x = \rho U\phi \qquad \text{and}$$

$$J_y = \rho V\phi - \Gamma_y(\partial\phi/\partial Y)$$

where U and V denote the dimensionless velocity components in the x and y directions. The symbol Γ denotes the diffusion coeffient. The control volume for the x-momentum equation was described by Patankar and Spalding, 1972. It is shown on the shaded portion in Fig. (C.2).

To obtain the finite difference in the x-momentum equation, we must first integrate Equation (C.4) over the control volume shown in Fig. (C.2).

$$\iint \frac{\partial J_x}{\partial X} dXdY + \iint \frac{\partial J_y}{\partial Y} dXdY = - \iint \frac{\partial \bar{P}}{\partial X} dXdY + \iint (\theta - \theta_\infty) dXdY \qquad (C.5)$$

Equation (C.5) can also be written as

$$\iint \partial J_x dY + \iint \partial J_y dX = -\iint \partial \bar{P} dY + \iint (\theta - \theta_\infty) dX dY \qquad (C.6)$$

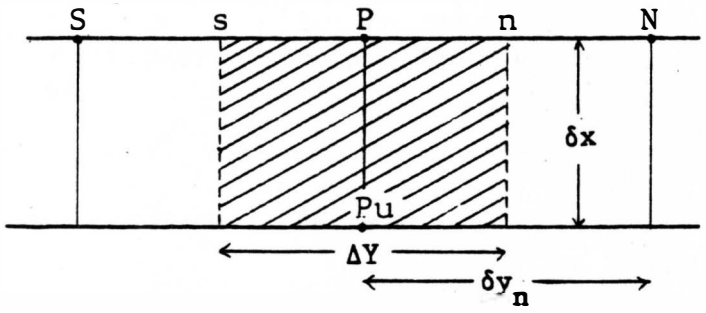

Fig. (C.2) Control volume (shaded) for two-dimensional flow

Dividing equation (C.6) by dX gives:

$$\iint \frac{\partial J_x}{\partial X} dY + \int \partial J_y = -\iint \frac{\partial \bar{P}}{\partial X} dY + \iint (\theta - \vartheta_\infty) dY \qquad (C.7)$$

Equation (C.7) is then integrated to give:

$$\left[\frac{J_{x,P} - J_{x,Pu}}{\delta x}\right] \Delta Y + (J_{y,n} - J_{y,s}) = -\frac{d\bar{P}}{dX} \Delta Y$$

$$+ (\theta - \theta_\infty) \Delta Y \qquad (C.8)$$

Next, one integrates the continuity equation over the same control volume.

$$\frac{\partial}{\partial X}(\rho U) + \frac{\partial}{\partial Y}(\rho V) = 0 \tag{C.9}$$

$$\iint \frac{\partial}{\partial X}(\rho U)dXdY + \iint \frac{\partial}{\partial Y}(\rho V)dXdY = 0 \tag{C.10}$$

Equation (C.10) can be written as

$$\iint \partial(\rho U)dY + \iint \partial(\rho V)dX = 0 \tag{C.11}$$

Dividing equation (C.11) by dX

$$\iint \frac{d}{dX}(\rho U)dY + \iint d(\rho V) = 0 \tag{C.12}$$

and integrating results in:

$$\left[\frac{(\rho U)_{x,P} - (\rho U)_{x,Pu}}{\delta x}\right]\Delta Y + [(\rho V)_{y,n} - (\rho V)_{y,s}] = 0 \tag{C.13}$$

A new symbol F is defined as follows:

$$F \equiv \rho U \tag{C.14}$$

Equation (C.13) can be written as:

$$\left[\frac{F_{x,P} - F_{x,Pu}}{\delta x}\right]\Delta Y + (F_{y,n} - F_{y,s}) = 0 \qquad (C.15)$$

Multiplying equation (C.15) by ϕ_P gives

$$\left[\frac{F_{x,P} - F_{x,Pu}}{\delta x}\right]\phi_P\Delta Y + (F_{y,n}\phi_P - F_{y,s}\phi_P) = 0 \qquad (C.16)$$

where,

$$F_{x,P} = \rho U_{x,P} \quad , \quad F_{y,n} = \rho V_{y,n}$$

$$F_{x,Pu} = \rho U_{x,Pu} \quad , \quad F_{y,s} = \rho V_{y,s}$$

As mentioned earlier, the x-momentum equation must satisfy the continuity equation. This can be accomplished by subtracting the x-momentum equation (equation (C.8)) from the continuity equation (equation (C.16)), which gives

$$(J_{x,P} - F_{x,P}\phi_P)\frac{\Delta Y}{\delta x} + (F_{x,Pu}\phi_P - J_{x,Pu})\frac{\Delta Y}{\delta x} + (J_{y,n}$$

$$- F_{y,n}\phi_P) + (F_{y,s}\phi_P - J_{y,s}) = -\frac{d\bar{P}}{dX}\Delta Y$$

$$+ (\theta - \theta_\infty)\Delta Y \qquad (C.17)$$

But the first term on the right side of equation (C.17) is equal to zero while the third and fourth terms are expressed as follows:

$$(J_{y,n} - F_{y,n}\phi_P) = a_n(\phi_P - \phi_N) \tag{C.18}$$

$$(J_{y,s} - F_{y,s}\phi_P) = a_s(\phi_S - \phi_P) \tag{C.19}$$

thus, equation (C.17) becomes

$$(F_{x,Pu} - J_{x,Pu})\frac{\Delta Y}{\delta x} + a_n(\phi_P - \phi_N) - a_s(\phi_S - \phi_P) =$$

$$- \frac{d\bar{P}}{dX}\Delta Y + (\theta - \theta_\infty)\Delta Y \tag{C.20}$$

The discretization equation (C.20) can be arranged more compactly as shown below

$$a_P\phi_P = a_n\phi_N + a_s\phi_S + J_{x,Pu}\frac{\Delta Y}{\delta x} - \frac{d\bar{P}}{dX}\Delta Y + (\theta - \theta_\infty)\Delta Y \tag{C.21}$$

where,

$$a_P = a_n + a_s + F_{x,Pu}\frac{\Delta Y}{\delta x} \tag{C.22a}$$

$$a_n = D_n A(|P_n|) + [\![-F_{y,n}\ ,\ 0]\!] \tag{C.22b}$$

$$a_s = D_s A(|P_s|) + [\![\ F_{y,s}\ ,\ 0]\!] \tag{C.22c}$$

$$F_{x,Pu} = \rho U_{Pu} \quad , \quad J_{x,Pu} = F_{x,Pu}\phi_{Pu} \tag{C.22d}$$

$$D_n = \Gamma/\delta y_n \quad , \quad D_n = \Gamma/\delta y_s \tag{C.22e}$$

$$P_n = F_{y,n}/D_n \quad , \quad P_s = F_{y,s}/D_s \tag{C.22f}$$

$$F_{y,n} = \rho V_n \quad , \quad F_{y,s} = \rho V_s \tag{C.22g}$$

and

$$D \equiv \Gamma/\delta_s \tag{C.23a}$$

$$A(|P_s|) = |P_s|/[\exp(|P_s|)-1] \tag{C.23b}$$

Note: The function A(|P|) can be obtained from table 5.2 of Patankar, 1980.

The Newton-Raphson function is used to correct for the mean pressure gradient and also for the mean velocity in the x-direction. The Newton-Raphson function is obtained by taking the derivative of equation (C.22) with respect to $-(d\bar{P}/dX)$. A new symbol Z is introduced, where Z is defined as:

$$Z \equiv -(d\bar{P}/dX) \tag{C.24}$$

Taking the derivative of equation (C.21) one has:

$$a_P \frac{dU_P}{dZ} = a_n \frac{dU_n}{dZ} + a_s \frac{dU_s}{dZ} + 0 + 1\Delta Y + 0 \tag{C.25}$$

Let the new symbol r be defined as

$$r \equiv dU/dZ \qquad (C.26)$$

Then, equation (C.25) becomes:

$$a_P r_P = a_n r_n + a_s r_s + \Delta Y \qquad (C.27)$$

Finite difference method for the y-Momentum Equation

To obtain the finite difference in the y-momentum equation, the control volume is staggered in the y-direction. This is described in Patankar, S.V. (Numerical Heat TRansfers, Hemisphere publication, 1980). The staggered control volume is shown in Fig.(C.3) on the shaded area.

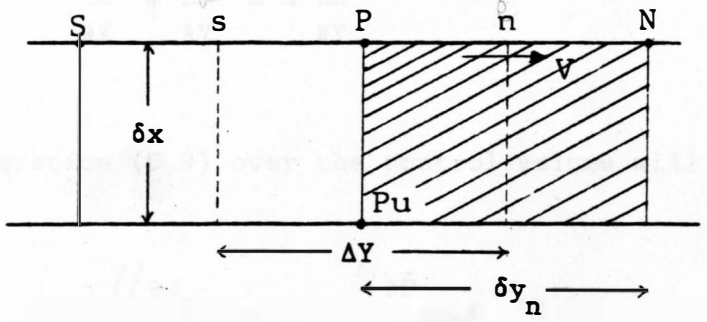

Fig.(C.3) Control volume (Shaded) at staggered location

If we focus attention on the location for V only, there is nothing unusual about this control volume. The control volume is staggered in

relation to the normal control volume at the main grid point P. The staggering is in the y-direction only, such that the grid points P and N are now on the control surfaces. The layout realizes one of the main advantages of the staggered grid: The difference $P_P - P_N$ can be used to calculate the pressure force acting on the control volume for the velocity V.

The location of V are shown in Fig C.3 by short arrows, while the grid points are shown by small circles. From Appendix A, the y-momentum equation is written as:

$$U\frac{\partial V}{\partial X} + V\frac{\partial V}{\partial Y} = -\frac{\partial \hat{P}}{\partial Y} + \frac{\partial^2 V}{\partial Y^2} \qquad (C.28)$$

Again, equation (C.28) can be written as

$$\frac{\partial J_x}{\partial X} + \frac{\partial J_y}{\partial Y} = -\frac{\partial \hat{P}}{\partial Y} \qquad (C.29)$$

Integrating equation (C.9) over the control volume will give

$$\iint \frac{\partial J_x}{\partial X} dX dY + \iint \frac{\partial J_y}{\partial Y} dX dY = -\iint \frac{\partial \hat{P}}{\partial Y} dX dY \qquad (C.30a)$$

Equation (C.30a) then reduces to

$$\iint \partial J_x dY + \iint \partial J_y dY = -\iint d\hat{P} dX \qquad (C.30b)$$

Rearranging equation (C.30b) gives

$$\iint \frac{\partial J_x}{\partial X} dY + \iint dJ_y = - \iint d\hat{P} \qquad \text{(C.30c)}$$

Thus, the integration of equation (C.29) over the control volume shown in Fig. C.3 (Shaded) can finally be written as:

$$\left[\frac{J_{x,n} - J_{x,nu}}{\delta x}\right] \delta y + (J_{y,N} - J_{y,P}) = \hat{P}_P - \hat{P}_N \qquad \text{(C.31)}$$

Integrating the continuity equation over the staggered control volume gives

$$\iint \partial(\rho U) dY + \iint \partial(\rho V) dX = 0 \qquad \text{(C.32a)}$$

Rearranging equation (C.32a), one gets

$$\iint \frac{d(\rho U)}{dX} dY + \iint d(\rho V) = 0 \qquad \text{(C.32b)}$$

Equation (C.32b) can also be written as

$$\left[\frac{\rho U_{x,n} - F_{x,nu}}{\delta x}\right] \delta y + (\rho V_{y,N} - \rho V_{y,P}) = 0 \qquad \text{(C.32c)}$$

or

$$\left[\frac{F_{x,n} - F_{x,nu}}{\delta x}\right]\delta y + F_{y,N} - F_{u,P} = 0 \qquad (C.33)$$

where

$$F_{x,n} = \rho U_{x,n} \quad , \quad F_{y,N} = \rho V_{y,N}$$

$$F_{x,nu} = \rho U_{x,nu} \quad , \quad F_{y,P} = \rho V_{y,P}$$

Multiplying equation (C.33) by ϕ one has:

$$\left[\frac{F_{x,n} - F_{x,nu}}{\delta x}\right]\phi_n\delta_y + F_{y,N}\phi_n - F_{y,P}\phi_n = 0 \qquad (C.34)$$

Subtracting the y-momentum equation (equation C.31) from the continuity equation (Equation C.34 one gets:

$$(F_{x,nu}\phi_n - J_{x,nu})\frac{\delta y}{\delta x} + a_N(\phi_n - \phi_{nn}) - a_P(\phi_s - \phi_n) =$$

$$\hat{P}_P - \hat{P}_N \qquad (C.35)$$

In a more compact form, equation (C.35) can be written as

$$b_n\phi_n = b_N\phi_{nn} + b_P\phi_s + J_{x,nu}\frac{\delta y}{\delta x} + \hat{P}_P - \hat{P}_N \qquad (C.36)$$

where

$$b_n = b_N + b_P + F_{x,nu}(\delta y/\delta x) \qquad \text{(C.37a)}$$

$$b_N = D_N A(|P_N|) + [\![- F_N, 0]\!] \qquad \text{(C.37b)}$$

$$b_P = D_P A(|P_P|) + [\![F_P, 0]\!] \qquad \text{(C.37c)}$$

$$D_N = (\Gamma_N/\Delta Y_N) \quad , \quad D_P = (\Gamma_P/\Delta Y_P) \qquad \text{(C.37d)}$$

$$P_N = (F_N/D_N) \quad , \quad P_P = (F_P/D_P) \qquad \text{(C.37e)}$$

$$F_N = \rho V_N \quad , \quad F_P = \rho V_P \qquad \text{(C.37f)}$$

$$F_{x,nu} = \rho U_{nu} \quad , \quad J_{x,nu} = \rho U_{nu} \phi_{nu} \qquad \text{(C.37g)}$$

Finite difference method for the Energy Equation

The control volume for the energy equation is shown in Fig (C.4) which is also similar to the control volume used for the x-momentum equation.

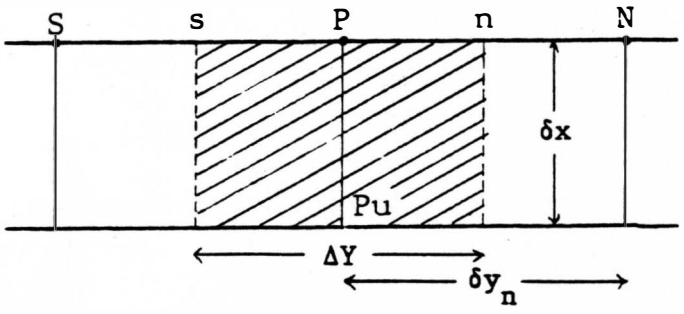

Fig. (C.4) Control volume for the energy equation.

As derived in Appendix A, the energy equation is

$$U\frac{\partial\theta}{\partial X} + V\frac{\partial\theta}{\partial Y} = \frac{1}{Pr}\frac{\partial^2\theta}{\partial Y^2} \qquad (C.38)$$

Equation (C.38) can be written as

$$\frac{\partial J_x}{\partial X} + \frac{\partial J_y}{\partial Y} = 0 \qquad (C.39)$$

where

$$J_x = \rho U \phi \tag{C.40a}$$

$$J_y = \rho V \phi - \Gamma_y (d\phi/dY) \tag{C.40b}$$

$$\Gamma_y = 1/Pr \tag{C.40c}$$

Integrating equation (C.39) over the shaded control volume shown in Fig. (C.4).

$$\iint \frac{\partial J_x}{\partial X} dX dY + \iint \frac{\partial J_y}{\partial Y} dX dY = 0 \tag{C.41}$$

or by rearranging:

$$\iint \frac{\partial J_x}{\partial X} dY + \iint dJ_y = 0 \tag{C.42}$$

According to the shaded control volume shown in Fig. C.4, equation (C.42) is written as

$$\left[\frac{J_{x,P} - J_{x,Pu}}{\delta x}\right] \delta y + J_{y,n} - J_{y,s} = 0 \tag{C.43}$$

Subtracting the energy equation (equation C.43) from the continuity equation (equation C.16) gives:

$$(J_{x,P} - F_{x,P}\phi_P)\frac{\Delta Y}{\delta x} + (F_{x,Pu}\phi_P - J_{x,Pu})\frac{\Delta Y}{\delta x} + (J_{y,n} - F_{y,n}\phi_P)$$

$$+ (F_{y,s}\phi_P - J_{y,s}) = 0 \qquad (C.44)$$

The first term in equation (C.44) will vanish so that one gets:

$$(F_{x,Pu}\phi_P - J_{x,Pu})\frac{\Delta Y}{\delta x} + (J_{y,n} - F_{y,s}\phi_P)$$

$$+ (F_{y,s}\phi_P - J_{y,s}) = 0 \qquad (C.45)$$

or

$$(F_{x,Pu}\phi_P - J_{x,Pu})\frac{\Delta Y}{\delta x} + a_n(\phi_P - \phi_N) - a_s(\phi_S - \phi_P) = 0 \qquad (C.46)$$

In a more compact form, equation (C.46) is expressed as

$$C_P\phi_P = C_n\phi_N + C_s\phi_S + J_{x,Pu}(\Delta Y/\delta x) \qquad (C.47)$$

where

$$C_P = C_n + C_s + F_{x,Pu}(\Delta Y/\delta x) \qquad (C.48a)$$

$$C_n = D_n A(|P_n|) + [\![- F_{y,n} , 0]\!] \qquad (C.48b)$$

$$C_s = D_s A(|P_s|) + [\![F_{y,s} , 0]\!] \qquad (C.48c)$$

$$D_n = \Gamma/\delta y_n \quad , \quad D_s = \Gamma/\delta y_s \tag{C.48d}$$

$$P_n = F_{y,n}/D_n \quad , \quad P_s = F_{y,s}/D_s \tag{C.48e}$$

$$F_{y,n} = \rho V_n \quad , \quad F_{y,s} = \rho V_s \tag{C.48f}$$

$$F_{x,Pu} = \rho U_{Pu} \quad , \quad J_{x,Pu} = F_{x,Pu}\phi_{Pu} \tag{C.48g}$$

PRESSURE EQUATION

The equation for pressure is obtained by introducing the velocity correction suggested by Patankar and Spalding to the continuity equation. It is done as follows:

Continuity equation

$$\frac{\partial U}{\partial X} + \frac{\partial V}{\partial Y} = 0 \tag{C.49}$$

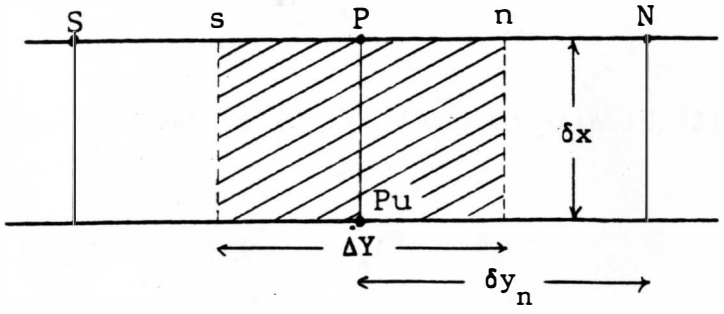

Fig. (C.5) Control volume for the Pressure equation

First, integrating equation (C.49) over the control volume, one gets:

$$\int\int \frac{\partial}{\partial X}(\rho U)dXdY + \int\int \frac{\partial}{\partial Y}(\rho V)dXdY = 0 \qquad (C.50)$$

Equation (C.50) can also be written as

$$\int\int \partial(\rho U)dY + \int\int \partial(\rho V)dX = 0 \qquad (C.51)$$

Referring to Fig. (C.5), equation (C.51) gives

$$(\rho U_P - \rho U_{Pu})\Delta Y + (\rho V_n - \rho V_s)\delta x = 0 \qquad (C.52)$$

Introducing the velocity correction equation as mentioned by Patankar and Spalding,

$$V_n = \hat{V}_n + \phi_n(\hat{P}_P - \hat{P}_N) \qquad (C.53a)$$

$$V_s = \hat{V}_s + \phi_s(\hat{P}_S - \hat{P}_P) \qquad (C.53b)$$

and substituting equation (C.53a - C.53b) into (C.52), gives

$$[(\rho U)_P - (\rho U)_{Pu}]\Delta Y + [\rho(\hat{V}_n + \phi_n(\hat{P}_P - \hat{P}_N)) - \rho(\hat{V}_s + d_s(\hat{P}_S - \hat{P}_P))]\delta x = 0 \qquad (C.54)$$

Equation (C.54) can be simplified to give

$$\rho U_{Pu}\left[\frac{U_P}{U_{Pu}} - 1\right]\frac{\Delta Y}{\delta x} + [(\rho\hat{V})_n + \rho_n\phi_n(\hat{P}_P - \hat{P}_N)$$

$$- (\rho\hat{V})_s - \rho_s d_s(\hat{P}_S - \hat{P}_P)] = 0 \qquad (C.55)$$

Equation (C.55) can be written more compactly as follows

$$a_P''P_P = a_N''P_N + a_S''P_S + b'' \qquad (C.56)$$

where

$$a_P'' = a_N'' + a_S'' \qquad (C.57a)$$

$$a_N'' = \rho_n d_N \qquad (C.57b)$$

$$a_S'' = \rho_s d_S \qquad (C.57c)$$

$$b'' = L_s - L_n - F_{Pu}(U_P/U_{Pu} - 1) \qquad (C.57d)$$

$$F_{Pu} = \frac{\Delta Y}{\delta x}(\rho V)_{Pu} \qquad (C.57e)$$

$$L_n = \rho_n\hat{V}_n \quad , \quad L_s = \rho_s\hat{V}_s \qquad (C.57f)$$

$$d_N = 1/a_N' \quad , \quad d_S = 1/a_S' \qquad (C.57g)$$

It should be noted that b'' in the pressure equation is essentially the left-hand side of the discretized continuity equation (C.45) evaluated in terms of the starred velocities. If b'' is zero,

it means that no pressure correction is needed. If not, the following equation is obtained for the pressure correction,

$$a_P"P_P' = a_n"P_N' + a_sP_S' + b' \tag{C.59}$$

where

$$b' = L_s - L_n - F_{Pu}(U_P/U_{Pu} - 1) \tag{C.60}$$

APPENDIX D

Linearization procedure of the radiative terms.

APPENDIX D

LINEARIZATION EQUATION

This appendix is on the linearization of θ^4 radiative term by employing Taylor series.

For the interaction of radiation and convection, the thermal boundary condition is non-linear. The temperature 'θ', term is of the fourth order. Thus, we must linearize it. One may linearize θ by applying Taylor series. Taylor series state that

$$f_n(x) = f(x_o) + f'(x_o)(x - x_o) + \frac{f''(x_o)}{2!}(x - x_o)^2 + \ldots + \frac{f''(x_o)}{n!}(x - x_o)^n \qquad (D.1)$$

The linearization of the θ term in the thermal boundary condition (equation B.23 & B.24) can thus be obtained as follows:

$$\theta^4 = \theta^{*4} + 4\theta^{*3}(\theta - \theta^*) \qquad (D.2)$$

Note that equation (D.2) can be further simplified to give

$$\theta^4 = 4\theta^{*3}\theta - 3\theta^{*4} \qquad (D.3)$$

Where θ^* is the previous-iteration value of θ .

APPENDIX E

Solution of the linear algebraic equations.

APPENDIX E

SOLUTION OF THE LINEAR ALGEBRAIC EQUATION

The solution of the discretization equations is discussed in Patankar, 1980. It is obtained using the TriDiagonal-Matrix Algorithm (TDMA).

Considering the control volume (Figure E.1) in order to present the algorithm,

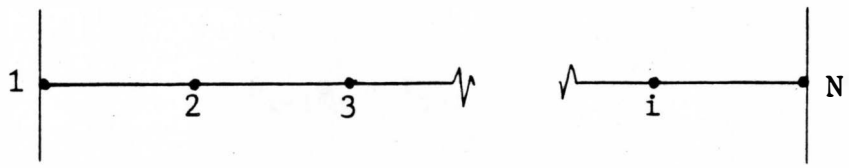

Fig. (E.1)

the discretization equation is written as:

$$b_i \phi_i = c_i \phi_{i+1} + a_i \phi_{i-1} + d_i \qquad \text{(E.1)}$$

Rearranging the above equation gives

$$- a_i \phi_{i-1} + b_i \phi_i - c_i \phi_{i+1} = d_i \qquad \text{(E.2)}$$

The computer program is written in such a way that the input value of the coefficient a_i and c_i are both negative. Thus, equation (E.2) can be written as

$$a_i\phi_{i-1} + b_i\phi_i + c_i\phi_{i+1} = d_i \tag{E.3}$$

But for the forward-substitution process, the relationship between ϕ_i and ϕ_{i+1} can be written as follows:

$$\phi_i = \beta_i\phi_{i+1} + \gamma_i \tag{E.4}$$

Thus

$$\phi_{i-1} = \beta_{i-1}\phi_i + \gamma_{i-1} \tag{E.5}$$

Substituting equation (E.5) into (E.3), gives

$$\phi_i = \frac{-c_i\phi_{i+1}}{b_i + a_i\beta_{i-1}} + \frac{d_i - a_i\gamma_{i-1}}{b_i + a_i\beta_{i-1}} \tag{E.6}$$

Note that the first value of β_1 and γ_1 are given as b_1 and d_1/β_1 respectively. Equation (E.6) can now be reduced to:

$$\phi_i = \frac{-c_i\phi_{i+1}}{\beta_i} + \gamma_i \tag{E.7}$$

where

$$\beta_i = b_i - \frac{a_i c_{i-1}}{\beta_{i-1}} ,$$

$$\gamma_i = \frac{d_i - a_i \gamma_{i-1}}{\beta_i} \qquad \text{(E.8)}$$

APPENDIX F

Derivation of the view factors.

APPENDIX F

VIEW FACTOR

The "crossed-string" method of Hottel is used to calculate the view factor between surfaces that are of infinite extent in one direction. For two such surfaces, Fig. (F.1) with unobstructed views of one another, the view factor is of the form

$$F_{1-2} = \frac{1}{2W_1}((ac + bd) - (ad + bc)) \qquad (F.1)$$

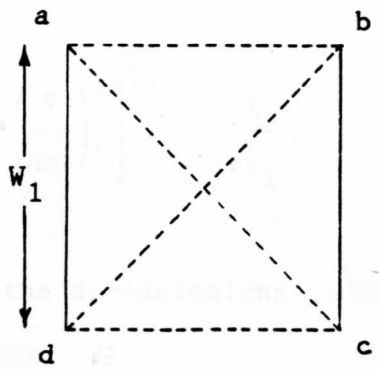

Fig. (F.1)

By using Equation (F.1), the view factor of the parallel plate channel of the present study can be solved. Note that the surfaces of the channel are divided into elements. Thus a view factor has to be calculated between each element and the rest of the elements on the opposing surface. Attention should be turned to the

figures shown below.

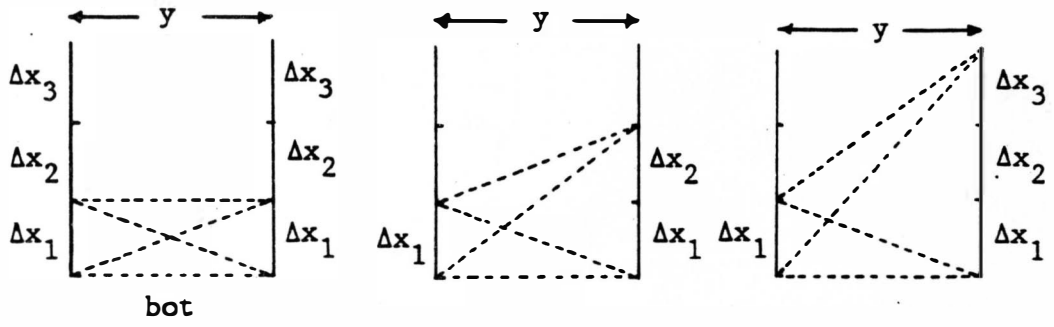

Fig. (F.2) (a) (b) (c)

The view factor from element Δx_1 to the element Δx_1 of the opposing surface can be written as

$$F_{1-1} = \left[1 + \left(\frac{y}{\Delta x_1}\right)^2\right]^{1/2} - \frac{y}{\Delta x_1} \qquad (F.2)$$

Introducing the dimensionless quantity (equation A.17a) into equation (F.2) will give:

$$F_{1-1} = \left[1 + \left(\frac{1}{\Delta X_1 Gr^*}\right)^2\right]^{1/2} - \frac{1}{\Delta X_1 Gr^*} \qquad (F.3)$$

From Fig. (F.2b), the view factor from element Δx_1 to the element Δx_1 and Δx_2 of the opposing surface is as follows

$$F_{1-1,2} = \frac{1}{2}\left[\left[\left(\frac{\Delta x_1 + \Delta x_2}{\Delta x_1}\right)^2 + \left(\frac{y}{\Delta x_1}\right)^2\right]^{1/2} + \left[1 + \left(\frac{y}{\Delta x_1}\right)^2\right]^{1/2} - \frac{y}{\Delta x_1} - \left[\left(\frac{\Delta x_2}{\Delta x_1}\right)^2 + \left(\frac{y}{\Delta x_1}\right)^2\right]^{1/2}\right] \quad (F.4)$$

Equation (F.4) can also be written as

$$F_{1-1,2} = \frac{1}{2}\left[\left[\left(\frac{\Delta X_1 + \Delta X_2}{\Delta X_1}\right)^2 + \left(\frac{1}{\Delta X_1 Gr^*}\right)^2\right]^{1\ 2} + \left[1 + \left(\frac{1}{\Delta X_1}\right)^2\right]^{1\ 2} - \left(\frac{1}{\Delta X_1 Gr^*}\right) - \left|\left(\frac{\Delta X_2}{\Delta X_1}\right)^2 + \left(\frac{1}{\Delta X_1 Gr^*}\right)^2\right]^{1\ 2}\right] \quad (F.5)$$

Finally, the view factor from element Δx_1 to the element Δx_2 of the opposing surface can be found by employing the decomposition rule as shown below.

$$F_{1-2} = F_{1-1,2} - F_{1-1} \quad (F.6)$$

Similarly,

$$F_{1-3} = F_{1-1,2,3} - F_{1-1,2} \quad (F.7)$$

From Fig. G.3b, the view factor $F_{bot-1,2}$ can be written as

$$F_{bot-1,2} = \frac{1}{2}\left[\frac{\Delta x_1 + \Delta x_2}{y} + 1 - \left[\left(\frac{\Delta x_1 + \Delta x_2}{y}\right)^2 + 1\right]^{1/2}\right] \qquad (F.10)$$

Introducing the dimensionless parameters (equation A.17b) to equation (F.10), gives

$$F_{bot-1,2} = 1/2\left[(\Delta X_1 + \Delta X_2)Gr^* + 1 - \left[((\Delta X_1 + \Delta X_2)Gr^*)^2 + 1\right]^{1/2}\right] \qquad (F.11)$$

Thus, the view factor from the inlet plane to the second surface element is as follow

$$F_{bot-2} = F_{bot-1,2} - F_{bot-1} \qquad (F.12)$$

Similarly,

$$F_{bot-3} = F_{bot-1,2,3} - F_{bot-1,2} \qquad (F.13)$$

Finally, the view factor between the inlet plane and the exit plane can be written as

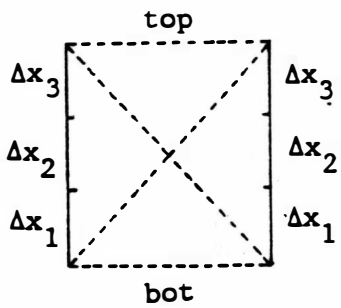

Fig. (G.4)

$$F_{bot\text{-}top} = \left[\left(\frac{\Delta x_1 + \Delta x_2 + \Delta x_3}{y}\right)^2 + 1\right]^{1/2} - \frac{\Delta x_1 + \Delta x_2 + \Delta x_3}{y} \qquad (F.14)$$

Substituting the dimensionless parameter (equation A.17a) into equation (F.14) gives

$$F_{bot\text{-}top} = \left[(\Delta X_1 + \Delta X_2 + \Delta X_3)Gr^* + 1\right]^{1/2} - (\Delta X_1 + \Delta X_2 + \Delta X_3)Gr^* \qquad (F.15)$$

APPENDIX G

Flow chart.

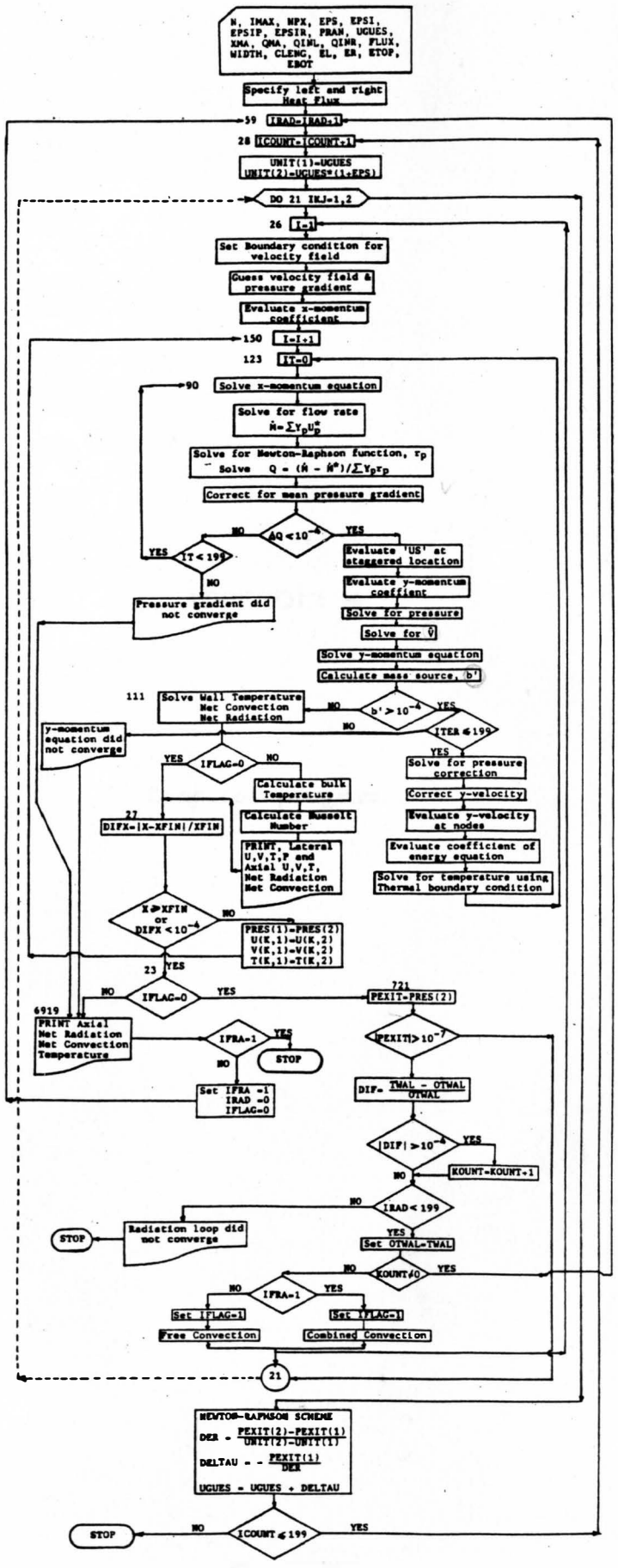
N, IMAX, NPX, EPS, EPSI, EPSIP, EPSIR, PRAN, UGUES, XMA, QNA, QINL, QINR, FLUX, WIDTH, CLENG, EL, ER, ETOP, EBOT
Specify left and right Heat Flux
59 IRAD=IRAD+1
28 ICOUNT=ICOUNT+1
UNIT(1)=UGUES
UNIT(2)=UGUES*(1+EPS)
DO 21 IKJ=1,2
26 I=1
Set Boundary condition for velocity field
Guess velocity field & pressure gradient
Evaluate x-momentum coefficient
150 I=I+1
123 IT=0
90 Solve x-momentum equation
Solve for flow rate
Solve for Newton-Raphson function, r_p
Solve $Q = (\dot{M} - \dot{M}^*)/\Sigma Y_p r_p$
Correct for mean pressure gradient
ΔQ < 10^-4
NO
YES
IT < 199
YES
NO
Pressure gradient did not converge
Evaluate 'US' at steggered location
Evaluate y-momentum coeffient
Solve for pressure
Solve for V̄
Solve y-momentum equation
Calculate mass source, b'
111 Solve Wall Temperature
Net Convection
Net Radiation
b' > 10^-4
NO
YES
y-momentum equation did not converge
ITER ≤ 199
YES
NO
IFLAG=0
YES
NO
Calculate bulk Temperature
Calculate Nusselt Number
27 DIFX=|X-XFIN|/XFIN
PRINT, Lateral U,V,T,P and Axial U,V,T, Net Radiation Net Convection
X ≥ XFIN or DIFX < 10^-4
NO
YES
PRES(1)=PRES(2)
U(K,1)=U(K,2)
V(K,1)=V(K,2)
T(K,1)=T(K,2)
23
IFLAG=0
NO
YES
6919 PRINT Axial Net Radiation Net Convection Temperature
IFRA=1
YES
NO
STOP
Set IFRA =1
IRAD =0
IFLAG=0
Solve for pressure correction
Correct y-velocity
Evaluate y-velocity at nodes
Evaluate coefficient of energy equation
Solve for temperature using Thermal boundary condition
721 PEXIT=PRES(2)
|PEXIT| > 10^-7
DIF= (TWAL - OTWAL)/OTWAL
|DIF| > 10^-4
YES
NO
KOUNT=KOUNT+1
IRAD < 199
NO
YES
STOP
Radiation loop did not converge
Set OTWAL=TWAL
KOUNT≠0
NO
YES
IFRA=1
NO
YES
Set IFLAG=1
Set IFLAG=1
Free Convection
Combined Convection
21
NEWTON-RAPHSON SCHEME
DER = (PEXIT(2)-PEXIT(1))/(UNIT(2)-UNIT(1))
DELTAU = - PEXIT(1)/DER
UGUES = UGUES + DELTAU
STOP
NO
ICOUNT ≤ 199
YES

APPENDIX H

Computer program.

APPENDIX H

The program in this appendix is written in WATFIV for the combined effect of free convection and radiation

```
CC Free convection problem for a fixed channel length
CC  with radiation
CC Radiation loop following Carpenter, Briggs and Sernas
CC
CC Initial velocity is iterated so that pressure at exit
CC  goes to zero
CC Parabolized equations Spalding-Patankar program revised
CC  with Patankar's Power Law scheme -- Simpler algorithm
CC Patankar's practice B
CC Two-Dimensional free convection laminar flow in
CC  a channel
CC Both velocity and temperature developing
CC Asymmetric surface flux prescribed at left wall
CC   QRAT1=Q1/Q10,  QRAT2=Q2/Q10
CC Asymmetric surface flux prescribed at right wall
CC
      IMPLICIT REAL*8 (A-H,O-Z)
      REAL*8 AA(45),BB(45),CC(45),Y(45),DELTAY(45),
     1 DELY(45),DD(45),AAA(45),BBB(45),CCC(45),DDD(45)
      REAL*8 US(45,2),VS(45,2),U(45,2),V(45,2),P(45),
     1 PPR(45),T(45,2),VTIL(45)
      REAL*8 FU(45),FUL(45),ANL(45),ASL(45),RR(45),
     1 PRES(2),APL(45)
      REAL*8 FF(45),F(45),UINIT(2),PEXIT(2)
      REAL*8 DELTAX(45),TWAL(45,2),QNTOT(45,2),
     1 QNCON(45,2),QNRAD(45,2),OTWAL(45,2),
     2 SHAPE(45,2,45,2),E(45,2),TWALL(45,2),TR(45,2)
      COMMON NPX1,NPX
      FUNC(P)=DMAX1(0.0D0,(1.0D0-0.1D0*DABS(P))**5)
CC
CC    N     --- Number of grid in the lateral
CC               direction
CC    IMAX  --- Number of iteration
CC    NPX   --- Number of grid in the flow direction
CC    PRAN  --- Prandtl Number
CC    UGUES --- Guess X-Velocity (Dimensionless)
CC    FLUX  --- Reference flux (W/m**2)
CC    WIDTH --- Channel width ( m )
CC    CLENG --- Channel length ( m )
CC    EL    --- Emissivities for the left surface
CC    ER    --- Emissivities for the right surface
CC    ETOP  --- Emissivities for the exit plane
CC    EBOT  --- Emissivities for the bottom plane
```

```
CC
      READ (5,11) N,IMAX
      READ (5,42) NPX
      READ (5,12) EPS,EPSI,EPSIP,EPSIR
      READ (5,1) PRAN,UGUES
      READ (5,12) XMA,QMA,QINL,QINR
      READ (5,2) FLUX,WIDTH,CLENG
      READ (5,1) EL,ER
      READ (5,1) ETOP,EBOT
CC
CC Properties at ambient temperature in dimensional form
CC  AMBT  ------ Ambient temperature (Kelvin)
CC  COND  ------ Thermal conductivity (W/m.K)
CC  VISK  ------ Kenimatic viscocity (m**2/s)
CC  GRAV  ------ Gravitational constant (m/s**2)
CC  STEFB ------ Stefan-Boltzmann constant (W/m**2.K**4)
CC
      AMBT = 300.D0
      VISK = 15.89D-06
      COND = 26.3D-03
      GRAV = 9.8D0
      STEFB = 5.67D-08
CC
      N1=N+1
      N2=N+2
      N3=N+3
      NPX1=NPX-1
      NPX2=NPX-2
CC
      TINIT = COND*AMBT/(FLUX*WIDTH)
      GR = GRAV*FLUX*WIDTH**4/(AMBT*VISK**2*COND)
      RN = STEFB*FLUX**3*WIDTH**4/(COND**4)
      HLRIO = CLENG/WIDTH
      DO 8352 JK=1,NPX1
      E(JK,1) = EL
      E(JK,2) = ER
8352  CONTINUE
      E(NPX,1) = ETOP
      E(NPX,2) = EBOT
CC
1     FORMAT (2F15.0)
2     FORMAT (3F15.0)
11    FORMAT (2I3)
12    FORMAT (4F15.0)
42    FORMAT (I5)
      IFRA=0
      IRAD=0
      IFLAG=0
      ICOUNT=0
      GAMNS=1.0D0
      GAMTNS=1.0D0/PRAN
```

```
      PRES(1)=0.0D0
      RAY=GR*PRAN
      XFIN=HLRIO/GR
      H=XFIN/NPX1
      I=1
      WRITE (6,725)
725   FORMAT('1',4X,'SURFACE HEAT FLUX PRESCRIBED AT
     1LEFT WALL',/)
      WRITE (6,7225)
7225  FORMAT(' ',4X,'SURFACE HEAT FLUX PRESCRIBED AT
     1RIGHT WALL',/)
7224  WRITE (6,13) N3,NPX,XFIN,H,PRAN,EPSI,EPS,EPSIP,
     1EPSIR,IMAX
13    FORMAT(5X,'NO OF POINTS IN Y-DIR N3 = ',I4,5X,
     1'NO OF POINTS IN X-DIR NPX = ',I4,//,5X,'XFIN = '
     2,D15.8,5X,'INITIAL DELX = ',D11.4,//,5X,
     3'PRANDTL NO = ',F15.10,//,5X,'EPSI =',D14.7,6X
     4,'EPS =',D14.7,6X,'EPSIP =',D14.7,//,5X,'EPSIR = '
     5,D14.7,7X,'IMAX = ',I5,//)
      WRITE(6,16)FLUX,WIDTH,CLENG
16    FORMAT(' ',/,1X,'FLUX =',D13.6,3X,'WIDTH =',D13.6,
     1           /,1X,'LENGTH OF CHANNEL  =',D20.13,/)
      WRITE (6,18) XMA,QMA,QINL,QINR
18    FORMAT (5X,'XMA = ',F9.5,3X,'QMA = ',F9.5,3X,
     1'QINLEFT = ',F9.5,3X,'QINRIGHT = ',F9.5,//)
      WRITE(6,19)RN,TINIT,HLRIO,GR,RAY
19    FORMAT(' ',4X,'RADIATION NUMBER IS =',D15.8,3X,
     1'TINIT = ',D15.8,//,5X,'ASPECT RATIO (L/H) = ',
     2D10.3,//5X,'GRASHOF NUMBER = ',D13.6,3X,
     3'RAYLEIGH NUMBER = ',D13.6,///)
      DINT=1.0D0/N
      DELTAY(1)=0.0D0
      DELTAY(N3)=0.0D0
      DELTAY(2)=DINT/2.0D0
      DELTAY(N2)=DINT/2.0D0
      DO 10 K=3,N1
10    DELTAY(K)=DINT
      DO 15 K=1,N2
15    DELY(K)=(DELTAY(K)+DELTAY(K+1))/2.0D0
      Y(1)=0.0D0
      DO 20 K=2,N3
20    Y(K)=Y(K-1)+DELY(K-1)
      X=0.0D0
      DELTAX(1)=H/2+H
      DO 43 IK=2,NPX2
43    DELTAX(IK)=H
      DELTAX(NPX1)=H/2
      DO 444 IK=1,NPX1
444   WRITE(6,445)IK,DELTAX(IK)
445   FORMAT(/,5X,' DELTAX(',I2,') = ',D20.13)
      CALL VIEWFC(SHAPE,DELTAX,1.0D0,GR)
```

```
CC
CC    Specify boundary functions for total net heat
CC     flux at the boundaries
CC        Triangular variation
CC
      DELX=H
      DO 46 IK=1,NPX1
      DIF5=DABS(X-XMA)/XMA
      IF (X .GT. XMA .OR. DIF5 .LE. EPSI) GO TO 702
      QNTOT(IK,1)=QINL+QMA*(X+H)/XMA
      GO TO 703
 702  QNTOT(IK,1)=QINL-QMA*(X+H)/XMA+2.0D0*QMA
 703  QNTOT(IK,2)=0.0D0
CC
CC    Uniform conditions
CC
       QNTOT(IK,1)=1.0D0
       QNTOT(IK,2)=0.0D0
46    X=X+DELX
CC
CC Guess all of the wall temperarures and convective
CC  fluxes to the fluid
CC
      DO 144 IK=1,NPX1
      TWAL(IK,1)=TINIT
      TWAL(IK,2)=TINIT
      OTWAL(IK,1)=TWAL(IK,1)
      OTWAL(IK,2)=TWAL(IK,2)
      QNCON(IK,1)=QNTOT(IK,1)
144   QNCON(IK,2)=QNTOT(IK,2)
59    IRAD=IRAD+1
      ICOUNT=0
28    ICOUNT=ICOUNT+1
      UINIT(1)=UGUES
      UINIT(2)=UGUES*(1.0D0+EPS)
      DO 21 IKJ=1,2
26    I=1
      X=0.0D0
      PRES(1)=0.0D0
CC
CC    Set initial condition for velocity
CC
      DO 60 K=1,N3
      V(K,1)=0.0D0
60    U(K,1)=UINIT(IKJ)
      DO 65 K=1,N2
      US(K,1)=UINIT(IKJ)
      VTIL(K)=0.0D0
65    VS(K,1)=0.0D0
CC
CC    Set initial condition for temperature
```

```
CC
      DO 67 K=1,N3
67    T(K,1)=TINIT
      TWAL(NPX,1)=TINIT
      TWAL(NPX,2)=TINIT
CC
CC    Evaluate actual flow rate
CC
      FLOW=0.0D0
      DO 70 K=1,N3
70    FLOW=FLOW+U(K,1)*DELTAY(K)
CC
CC    Set boundary conditions for velocity field
CC
      U(1,2)=0.0D0
      U(N3,2)=0.0D0
      US(1,2)=0.0D0
      US(N2,2)=0.0D0
      VTIL(1)=0.0D0
      VTIL(N2)=0.0D0
      VS(1,2)=0.0D0
      V(1,2)=0.0D0
      VS(N2,2)=0.0D0
      V(N3,2)=0.0D0
CC
CC    Guess Velocity field for Y-Component
CC
      DO 77 K=2,N1
77    VS(K,2)=VS(K,1)
CC
CC       Evaluate Y-Velocity at nodes
CC
      DO 142 K=2,N2
142   V(K,2)=(VS(K-1,2)+VS(K,2))/2.0D0
CC
CC    Guess the mean pressure gradient
CC
      DPDX=-8.0D0
CC
CC      Guess temperature field
CC
      DO 143 K=1,N3
143   T(K,2)=T(K,1)
CC
CC    Evaluate coefficients for X-Momentum equation
CC
150   I=I+1
      DELX=H
      X=X+DELX
      ITER=0
123   IT=0
```

```
      DPDXG=DPDX
      DO 72 K=2,N2
      FU(K)=DELTAY(K)*U(K,1)/DELX
      FYN=VS(K,2)
      FYS=VS(K-1,2)
      DN=GAMNS/DELY(K)
      DS=GAMNS/DELY(K-1)
      PN=FYN/DN
      PS=FYS/DS
      ANL(K)=DN*FUNC(PN)+DMAX1(-FYN,0.0D0)
      ASL(K)=DS*FUNC(PS)+DMAX1(FYS,0.0D0)
72    APL(K)=ANL(K)+ASL(K)+FU(K)
CC
CC      Solve X-momentum equation
CC
      BB(1)=1.0D0
      CC(1)=0.0D0
      DD(1)=0.0D0
      DO 74 K=2,N2
      AA(K)=-ASL(K)
      BB(K)=APL(K)
74    CC(K)=-ANL(K)
90    DO 75 K=2,N2
75    DD(K)=FU(K)*U(K,1)-DPDX*DELTAY(K)+(T(K,2)-TINIT)
     1*DELTAY(K)
      AA(N3)=0.0D0
      BB(N3)=1.0D0
      DD(N3)=0.0D0
      CALL TRIDAG (1,N3,AA,BB,CC,DD,FF)
      DO 76 K=1,N3
76    U(K,2)=FF(K)
CC
CC       Solve for new flow rate
CC
      FLOWS=0.0D0
      DO 78 K=1,N3
78    FLOWS=FLOWS+DELTAY(K)*U(K,2)
CC
CC     Solve for Newton-Raphson function r_p
CC
      DO 80 K=2,N2
80    DD(K)=DELTAY(K)
      CALL TRIDAG (1,N3,AA,BB,CC,DD,RR)
CC    Find DQ
      SUMRR=0.0D0
      DO 81 K=1,N3
81    SUMRR=SUMRR+DELTAY(K)*RR(K)
      DQ=(FLOW-FLOWS)/SUMRR
CC
CC     Correct mean pressure gradient and silve
CC     for mean pressure
```

```
CC
      DPDX=DPDXG-DQ
      DPDXG=DPDX
      PRES(2)=PRES(1)+DPDX*DELX
      DO 82 K=2,N2
82    U(K,2)=U(K,2)+RR(K)*DQ
      IT=IT+1
      IF (DABS(DQ) .LE. EPSI) GO TO 85
      IF (IT .LE. IMAX) GO TO 90
      WRITE (6,180) IT,I,X,ICOUNT,IRAD
180   FORMAT (////,1X,
     1'ITERATIONS FOR PRESSURE GRADIENT DID NOT
     2 CONVERGE AFTER ',2X,I4,2X,'TIMES',//,3X,'I = '
     3 ,I5,4X,'X = ',D14.7,4X,'ICOUNT = ',I5,4X
     4 ,'IRAD = ',I5,//)
      GO TO 6919
CC
CC    Evaluate X-velocities at staggered locations
CC
85    DO 86 K=2,N1
86    US(K,2)=U(K,2)+(U(K+1,2)-U(K,2))*0.5D0*DELTAY(K)
     1/DELY(K)
CC
CC    Evaluate coefficients for Y-momentum equation
CC
      DO 92 K=2,N1
      FUL(K)=DELY(K)*US(K,1)/DELX
      FYN=V(K+1,2)
      FYP=V(K,2)
      DN=GAMNS/DELTAY(K+1)
      DP=GAMNS/DELTAY(K)
      PN=FYN/DN
      PP=FYP/DP
      ANL(K)=DN*FUNC(PN)+DMAX1(-FYN,0.0D0)
      ASL(K)=DP*FUNC(PP)+DMAX1(FYP,0.0D0)
92    APL(K)=ANL(K)+ASL(K)+FUL(K)
CC
CC       Solve for pressure
CC
      AAA(1)=0.0D0
      CCC(1)=-1.0D0/APL(2)
      BBB(1)=-AAA(1)-CCC(1)
      DO 101 K=2,N
      AAA(K)=-1.0D0/APL(K)
      CCC(K)=-1.0D0/APL(K+1)
101   BBB(K)=-AAA(K)-CCC(K)
      AAA(N1)=-1.0D0/APL(N1)
      CCC(N1)=0.0D0
      BBB(N1)=-AAA(N1)-CCC(N1)
CC
CC      Calculate Vtil velocity
```

```
CC
      DO 96 K=2,N1
96    VTIL(K)=(ANL(K)*VS(K+1,2)+ASL(K)*VS(K-1,2)
     1 + FUL(K)*VS(K,1))/APL(K)
      DO 103 K=1,N1
103   DD(K)=VTIL(K)-VTIL(K+1)-FU(K+1)*(U(K+1,2)/
     1 U(K+1,1)-1.0D0)
      CALL TRIDAG (1,N1,AAA,BBB,CCC,DD,FF)
      DO 104 K=2,N2
104   P(K)=FF(K-1)
CC
CC     Solve Y-momentum equation
CC
      BB(1)=1.0D0
      CC(1)=0.0D0
      DD(1)=0.0D0
      DO 105 K=2,N1
      AA(K)=-ASL(K)
      CC(K)=-ANL(K)
      BB(K)=APL(K)
105   DD(K)=FUL(K)*VS(K,1)+P(K)-P(K+1)
      AA(N2)=0.0D0
      BB(N2)=1.0D0
      DD(N2)=0.0D0
      CALL TRIDAG (1,N2,AA,BB,CC,DD,FF)
      DO 106 K=1,N2
106   VS(K,2)=FF(K)
CC
CC   Calculate the mass source for the pressure
CC   correction equation
CC
      DO 107 K=1,N1
107   DDD(K)=VS(K,2)-VS(K+1,2)-FU(K+1)*(U(K+1,2)/
     1 U(K+1,1)-1.0D0)
CC
CC       Check for convergence
CC
      ITER=ITER+1
      DO 108 K=1,N1
      DIFF=DABS(DDD(K))
      IF (DIFF .GT. EPSI) GO TO 110
108   CONTINUE
      GO TO 111
110   IF (ITER .LE. IMAX) GO TO 112
      WRITE (6,114) ITER,X,ICOUNT,IRAD
114   FORMAT (//,1X,
     1'ITERATIONS FOR Y-MOMENTUM EQUATION DID NOT CONVERGE
     2  AFTER ITER = ',2X,I4,2X,'TIMES AT X = ',F10.5
     3 ,3X,'ICOUNT = ',I5,3X,'IRAD = ',I5,//)
      WRITE (6,186) I,X
186   FORMAT (////,5X,'I = ',I3,3X,'X = ',D14.7,//,5X,
```

```
     1'Y LOCATION',10X,'X-VELOCITY',9X,'Y-VELOCITY',
     29X,'PRESSURE',9X,'DIFFERENCE',9X,'TEMPERATURE',//)
      DO 118 K=1,N3
118   WRITE (6,190) Y(K),U(K,2),VS(K,2),P(K),DDD(K),T(K,2)
190   FORMAT (1X,6(D16.9,5X))
      GO TO 6919
CC
CC       Solve for pressure correction P_p'
CC
112   CALL TRIDAG (1,N1,AAA,BBB,CCC,DDD,FF)
      DO 121 K=2,N2
121   PPR(K)=FF(K-1)
CC
CC        Correct the Y-Velocity
CC
      DO 122 K=2,N1
122   VS(K,2)=VS(K,2)+(PPR(K)-PPR(K+1))/APL(K)
CC
CC       Evaluate Y-Velocity at nodes
CC
      DO 113 K=2,N2
113   V(K,2)=(VS(K-1,2)+VS(K,2))/2.0D0
CC
CC       Solve for temperature
CC
      DO 141 K=2,N2
      FYN=VS(K,2)
      FYS=VS(K-1,2)
      DN=GAMTNS/DELY(K)
      DS=GAMTNS/DELY(K-1)
      PN=FYN/DN
      PS=FYS/DS
      ANL(K)=DN*FUNC(PN)+DMAX1(-FYN,0.0D0)
      ASL(K)=DS*FUNC(PS)+DMAX1(FYS,0.0D0)
141   APL(K)=ANL(K)+ASL(K)+FU(K)
      SUMRAD=0.0D0
      DO 901 IK=1,NPX1
901   SUMRAD=SUMRAD+SHAPE(I-1,1,IK,2)*((1.0D0-E(IK,2))*
     1 (QNCON(IK,2)-QNTOT(IK,2))/E(IK,2)+RN*TWAL(IK,2)**4)
      BB(1)=1.0D0+IFRA*DELY(1)*E(I-1,1)*RN*4.0D0
     1 *TWAL(I-1,1)**3
      CC(1)=-1.0D0
      DD(1)=DELY(1)*(QNTOT(I-1,1)+IFRA*E(I-1,1)*(RN*3.0D0
     1 *TWAL(I-1,1)**4+SHAPE(I-1,1,NPX,1)*RN*TINIT**4+
     2 SHAPE(I-1,1,NPX,2)*RN*TINIT**4+SUMRAD))
      DO 132 K=2,N2
      AA(K)=-ASL(K)
      BB(K)=APL(K)
      CC(K)=-ANL(K)
132   DD(K)=FU(K)*T(K,1)
      SUMRAD=0.0D0
```

```
      DO 902 IK=1,NPX1
902   SUMRAD=SUMRAD+SHAPE(I-1,2,IK,1)*((1.0D0-E(IK,1))*
     1 (QNCON(IK,1)-QNTOT(IK,1))/E(IK,1)+RN*TWAL(IK,1)**4)
      BB(N3)=1.0D0+IFRA*DELY(N2)*E(I-1,2)*RN**4.0D0
     1 *TWAL(I-1,2)**3
      AA(N3)=-1.0D0
      DD(N3)=DELY(N2)*(QNTOT(I-1,2)+IFRA*E(I-1,2)*(RN*3.0D0
     1 *TWAL(I-1,2)**4+SHAPE(I-1,2,NPX,1)*RN*TINIT**4+
     2 SHAPE(I-1,2,NPX,2)*RN*TINIT**4+SUMRAD))
      CALL TRIDAG (1,N3,AA,BB,CC,DD,FF)
      DO 136 K=1,N3
136   T(K,2)=FF(K)
      GO TO 123
CC
111   TWAL(I-1,1)=T(1,2)
      TWAL(I-1,2)=T(N3,2)
      QNCON(I-1,1)=-(T(2,2)-T(1,2))/DELY(1)
      QNCON(I-1,2)=(T(N3,2)-T(N2,2))/DELY(N2)
      QNRAD(I-1,1)=QNTOT(I-1,1)-QNCON(I-1,1)
      QNRAD(I-1,2)=QNTOT(I-1,2)-QNCON(I-1,2)
      IF (IFLAG .EQ. 0) GO TO 27
CC
CC     Calculate dimensionless bulk temperature
CC
      WRITE(6,491) ITER,IT,ICOUNT,IRAD,IFLAG,IFRA
491   FORMAT(/,5X,'SOLUTION CONVERGED AFTER ITER =',I4,
     12X,'ITERATIONS',10X,'IT =',I3,/,5X,'ICOUNT =',I3,
     24X'IRAD =',I3,4X,'IFLAG =',I3,4X,'IFRA =',I3,/)
      DO 505 K=1,N3
505   F(K)=U(K,2)*T(K,2)
      CALL TRAPEZ (DELY,F,THETBU,N2)
      THETB1=T(1,2)-THETBU
      THETB2=T(N3,2)-THETBU
CC
CC       Calculate Nusselt Numbers
CC
      ANUD1=2.0D0*QNCON(I-1,1)/THETB1
      ANUD2=2.0D0*QNCON(I-1,2)/THETB2
CC
CC       Output of results
CC
      WRITE(6,510)I,X,THETBU,ANUD1,ANUD2,DPDX,PRES(2)
     1 ,FLOW
510   FORMAT('1',5X,'I =',I3,5X,'X =',D14.7,5X,
     1'BULK TEMPERATURE = ',D13.6,//,
     25X,'NUSSELT NUMBER AT LEFT WALL =',D13.6,/,
     35X,'NUSSELT NUMBER AT RIGHT WALL =',D13.6,/,
     45X,'PRESSURE GRADIENT = ',D13.6,
     53X,'PRESSURE = ',D13.6,/,5X,'FLOW RATE = ',D13.6,/)
      WRITE (6,511) E(I-1,1),E(I-1,2),QNCON(I-1,1),
     1 QNRAD(I-1,1),QNTOT(I-1,1),QNTOT(I-1,2),QNCON(I-1,2)
```

```
     2 ,QNRAD(I-1,2)
511   FORMAT(' ',4X,'EMISSIVITY-LEFT = ',D15.8,6X,
     1'EMISSIVITY-RIGHT = ',D15.8,//,5X,
     2'QNCON-LE = ',D23.16,5X,'QNRAD-LE = ',D23.16,/,5X,
     3'QNTOT-LE = ',D23.16,5X,'QNTOT-RI = ',D23.16,/,5X,
     4'QNCON-RI = ',D23.16,5X,'QNRAD-RI = ',D23.16,//,
     56X,'Y LOCATION',6X,'X-VELOCITY',6X,'Y-VELOCITY',
     66X,'PRESSURE',8X,'TEMPERATURE',4X,'TWAL/TINIT',/)
      DO 515 K=1,N3
      TR(K,2)=T(K,2)/TINIT
515   WRITE(6,520) Y(K),U(K,2),V(K,2),P(K),T(K,2),TR(K,2)
520   FORMAT (' ',3X,D13.6,2X,3(D14.7,2X),D15.8,2X,D15.8)
27    DIFX=DABS(X-XFIN)/XFIN
      IF (X .GE. XFIN .OR. DIFX .LE. EPSI) GO TO 23
      PRES(1)=PRES(2)
      DO 145 K=1,N3
      U(K,1)=U(K,2)
      V(K,1)=V(K,2)
145   T(K,1)=T(K,2)
      DO 147 K=1,N2
      VS(K,1)=VS(K,2)
147   US(K,1)=US(K,2)
      GO TO 150
23    IF (IFLAG .EQ. 0) GO TO 721
6919  CONTINUE
CC         Print result at the axial location
      DO 2222 LK=1,2
      DO 2222 JK=1,NPX
2222  TWALL(JK,LK)=TWAL(JK,LK)/TINIT
      WRITE(6,55)
55    FORMAT('1',///,4X,' SURFACE',3X,'EMISS.'
     1 ,3X,'TWAL/TINIT',8X,'NET RAD.',8X,'NET CONV.'
     2 ,5X,'NET TOT.',//)
      DO 50 IKI=1,NPX1
      WRITE(6,51)IKI,E(IKI,1),TWALL(IKI,1)
     1,QNRAD(IKI,1),QNCON(IKI,1),QNTOT(IKI,1)
50    CONTINUE
51    FORMAT(' ',4X,'LEFT  ',I3,2X,F4.2,2X,3(D14.7,3X)
     1 ,F4.2)
      WRITE(6,5523)E(NPX,1),TWALL(NPX,1)
5523  FORMAT(' ',4X,'BOTTOM ',4X,F4.2,2X,D14.7)
      DO 5522 IKI=1,NPX1
      WRITE(6,54)IKI,E(IKI,2),TWALL(IKI,2)
     1 ,QNRAD(IKI,2),QNCON(IKI,2),QNTOT(IKI,2)
5522  CONTINUE
54    FORMAT(' ',4X,'RIGHT ',I3,2X,F4.2,2X,3(D14.7,3X)
     1 ,F4.2)
      WRITE(6,5524) E(NPX,2),TWALL(NPX,2)
5524  FORMAT(' ',4X,'TOP ',7X,F4.2,2X,D14.7)
      IF (IFRA .EQ. 1) STOP
      IFRA=1
```

```
      IRAD=0
      IFLAG=0
      GO TO 59
721   PEXIT(IKJ)=PRES(2)
      CHEK=PEXIT(IKJ)
      IF ( DABS(CHEK) .GT. EPSIP ) GOTO 21
CC
CC      Calculate average temperature at exit
CC
      DO 57 K=1,N3
57    F(K)=T(K,2)
      CALL TRAPEZ (DELY,F,AVERF,N2)
CC    TWAL(NPX,2)=AVERF
CC    TWAL(NPX,2)=TINIT
CC
CC    Check for convergence of radiation loop by
CC    comparing the wall temperatures
CC
      KOUNT=0
      DO 58 IM=1,2
      DO 58 IK=1,NPX1
      DIF=(TWAL(IK,IM)-OTWAL(IK,IM))/OTWAL(IK,IM)
58    IF (DABS(DIF) .GT.EPSIR) KOUNT=KOUNT+1
      IF (IRAD.LE.IMAX) GO TO 928
      WRITE (6,61) IRAD,IFRA,KOUNT,IFLAG
61    FORMAT ('1',2X,
     1'ITERATION FOR RADIATION LOOP DID NOT CONVERGE
     2AFTER IRAD = ',I5,'ITERATIONS',//,3X,'IFRA = ',I6,
     33X,'KOUNT = ',I6,2X,'IFLAG = ',I6,//,3X,'IK',13X,
     4'TWAL-LEFT',40X,'TWAL-RIGHT',/)
      DO 62 IK=1,NPX
      WRITE (6,63) IK,TWAL(IK,1),OTWAL(IK,1),TWAL(IK,2)
     1,OTWAL(IK,2)
62    CONTINUE
63    FORMAT (2X,I4,4(10X,D14.7))
      STOP
928   DO 929 IM=1,2
      DO 929 IK=1,NPX1
929   OTWAL(IK,IM)=TWAL(IK,IM)
      IF (KOUNT .NE. 0) GO TO 59
      IF (IFRA .EQ. 1) GO TO 906
      IFLAG=1
      WRITE (6,932) IKJ,UINIT(IKJ),CHEK,DELTAU
932   FORMAT ('1',20X,'PURE FREE CONVECTION',////,
     15X,'IKJ = ',I2,3X,'UINIT = ',D20.10,5X,'PEXIT = ',
     2D20.10,//,6X,'LAST CORRECTION = ',D14.7,////)
      GO TO 26
906   IFLAG=1
      WRITE (6,32) IKJ,UINIT(IKJ),CHEK,DELTAU
32    FORMAT ('1',20X,'COMBINED FREE CONVECTION WITH
     1 RADIATION',////,6X,'IKJ = ',I2,3X,'UINIT = ',
```

```
     2 D20.10,5X,'PEXIT = ',D20.10,//6X,
     3 'LAST CORRECTION = ',D14.7,///)
       GO TO 26
21     CONTINUE
CC
CC        Newton-Raphson Scheme
CC
       DER=(PEXIT(2)-PEXIT(1))/(UINIT(2)-UINIT(1))
       DELTAU=-PEXIT(1)/DER
       UGUES=UGUES+DELTAU
       IF (ICOUNT .LE. IMAX) GO TO 28
       WRITE (6,29) ICOUNT,IRAD,UGUES,DELTAU,PEXIT(1)
      1 ,PEXIT(2)
29     FORMAT ('1',1X,'ITERATION FOR INITIAL VELOCITY DID
      1NOT CONVERGE AFTER ICOUNT = ',I5,1X,'ITERATIONS'
      2,5X,'IRAD = ',I5,//,1X,'UGUES = ',D14.7,5X,
      3'DELTA U = ',D14.7,5X,'PEXIT(1) = ',D14.7,5X,
      4'PEXIT(2) = ',D14.7)
       STOP
       END
       SUBROUTINE TRIDAG(IF,L,A,B,C,D,V)
       IMPLICIT REAL*8 (A-H,O-Z)
       REAL*8 A(45),B(45),C(45),D(45),V(45),BETA(45)
      1 ,GAMMA(45)
       BETA(IF)=B(IF)
       GAMMA(IF)=D(IF)/BETA(IF)
       IFP1=IF+1
       DO 1 I=IFP1,L
       BETA(I)=B(I)-A(I)*C(I-1)/BETA(I-1)
1      GAMMA(I)=(D(I)-A(I)*GAMMA(I-1))/BETA(I)
       V(L)=GAMMA(L)
       LAST=L-IF
       DO 2 K=1,LAST
       I=L-K
2      V(I)=GAMMA(I)-C(I)*V(I+1)/BETA(I)
       RETURN
       END
       SUBROUTINE TRAPEZ(DX,F,SUM,N2)
       IMPLICIT REAL*8 (A-H,O-Z)
       REAL*8 DX(45),F(45)
       SUM=0.0D0
       DO 10 I=1,N2
10     SUM=SUM+0.5D0*(F(I)+F(I+1))*DX(I)
       RETURN
       END
CC
CC  This Subroutine can calculate the view factors
CC  between surfaces that are of infinite extent. It
CC  will also calculate the view factor between
CC  itself.
CC
```

```
      SUBROUTINE VIEWFC(SHAPE,DELTAX,H,GR)
      IMPLICIT REAL*8 (A-H,O-Z)
      REAL*8 SHAPE(45,2,45,2),DELTAX(45)
      COMMON NPX1,NPX
CC
      DFUNC(RDD,RDD1,RH1)=0.5D0*((1+(RH1*RH1))**0.5+
     1 (RDD*RDD+RH1*RH1)**0.5-(RDD1*RDD1+RH1*RH1)
     2 **0.5D0-RH1)
CC
CC Set zero shape factor
      DO 20 J=1,2
      DO 20 I=1,NPX
      DO 20 K=1,NPX
      SHAPE(K,J,I,J)=0.0D0
20    CONTINUE
CC Shape factor between side wall
      DO 30 I=1,NPX1
      DD  = 0.D0
      SUM = 0.D0
      DO 30 J=I,NPX1
      SUM1= SUM
      DD  = DD+DELTAX(J)
      DD1 = DD-DELTAX(I)
      RDD = DD/DELTAX(I)
      RDD1= DD1/DELTAX(I)
      RH1 = H/(DELTAX(I)*GR)
      SUM = DFUNC(RDD,RDD1,RH1)
      SHAPE(I,1,J,2)=SUM-SUM1
      SHAPE(I,2,J,1)=SHAPE(I,1,J,2)
30    CONTINUE
CC  Reciprocity relation between side wall
      DO 35 K=1,2
      DO 35 KK=1,2
      DO 35 J=1,NPX1
      DO 35 I=J,NPX1
      SHAPE(I,K,J,KK)=DELTAX(J)*SHAPE(J,KK,I,K)/DELTAX(I)
35    CONTINUE
CC Bottom to side and top to side
      TSUM= 0.D0
      BSUM= 0.D0
      BDD = 0.D0
      TDD = 0.D0
      DO 40 I=1,NPX1
      II=NPX1-I+1
      BSUM1= BSUM
      TSUM1= TSUM
      BDD  = BDD+DELTAX(I)*GR
      TDD  = TDD+DELTAX(II)*GR
      RH1  = BDD/H
      RH2  = TDD/H
      BSUM = 0.5D0*((1.D0+RH1)-(RH1*RH1+1)**0.5D0)
```

```
      TSUM = 0.5D0*((1.D0+RH2)-(RH2*RH2+1)**0.5D0)
      SHAPE(NPX,1,I,1) = BSUM-BSUM1
      SHAPE(NPX,1,I,2) = SHAPE(NPX,1,I,1)
      SHAPE(NPX,2,II,1)= TSUM-TSUM1
      SHAPE(NPX,2,II,2)= SHAPE(NPX,2,II,1)
40    CONTINUE
CC Reciprocity relation for bottom to side and top to side
      DO 60 K=1,2
      DO 60 J=1,2
      DO 60 I=1,NPX1
      SHAPE(I,J,NPX,K) = SHAPE(NPX,K,I,J)*(H/(DELTAX(I)*GR))
60    CONTINUE
CC Shape factor between top and bottom
      RDH = (BDD)/H
      SHAPE(NPX,1,NPX,2) = (RDH*RDH+1.D0)**0.5D0-RDH
      SHAPE(NPX,2,NPX,1) = SHAPE(NPX,1,NPX,2)
CC       Print the result of the shape factor
      WRITE(6,126)
126   FORMAT('1',6X,'SURFACE',15X,'SHAPE FACTOR',/)
      DO 127 J=1,NPX1
      DO 127 I=1,NPX1
      WRITE(6,128)J,I,SHAPE(J,1,I,1)
128   FORMAT(' ',4X,'LEFT ',I3,1X,'TO LEFT ',I3,4X,D20.13)
127   CONTINUE
      DO 129 J=1,NPX1
      DO 129 I=1,NPX1
      WRITE(6,130)J,I,SHAPE(J,1,I,2)
130   FORMAT(' ',4X,'LEFT ',I3,1X,'TO RIGHT',I3,4X,D20.13)
129   CONTINUE
      DO 131 J=1,NPX1
      DO 131 I=1,NPX1
      WRITE(6,132)J,I,SHAPE(J,2,I,1)
132   FORMAT(' ',4X,'RIGHT',I3,1X,'TO LEFT ',I3,4X,D20.13)
131   CONTINUE
      DO 133 J=1,NPX1
      DO 133 I=1,NPX1
      WRITE(6,134)J,I,SHAPE(J,2,I,2)
134   FORMAT(' ',4X,'RIGHT',I3,1X,'TO RIGHT',I3,4X,D20.13)
133   CONTINUE
      DO 136 I=1,NPX1
      WRITE(6,135)I,SHAPE(I,1,NPX,1)
135   FORMAT(' ',4X,'LEFT ',I3,1X,'TO BOTTOM',6X,D20.13)
136   CONTINUE
      DO 137 I=1,NPX1
      WRITE(6,138)I,SHAPE(I,2,NPX,1)
138   FORMAT(' ',4X,'RIGHT',I3,1X,'TO BOTTOM',6X,D20.13)
137   CONTINUE
      DO 139 I=1,NPX1
      WRITE(6,140)I,SHAPE(I,1,NPX,2)
140   FORMAT(' ',4X,'LEFT ',I3,1X,'TO TOP',9X,D20.13)
139   CONTINUE
```

```
      DO 142 I=1,NPX1
      WRITE(6,141)I,SHAPE(I,2,NPX,2)
141   FORMAT(' ',4X,'RIGHT',I3,1X,'TO TOP',9X,D20.13)
142   CONTINUE
      DO 146 I=1,NPX1
146   WRITE(6,147)I,SHAPE(NPX,1,I,1)
147   FORMAT(' ',4X,'BOTTOM TO LEFT',1X,I3,6X,D20.13)
      DO 148 I=1,NPX1
148   WRITE(6,149)I,SHAPE(NPX,1,I,2)
149   FORMAT(' ',4X,'BOTTOM TO RIGHT',I3,6X,D20.13)
      DO 150 I=1,NPX1
150   WRITE(6,151)I,SHAPE(NPX,2,I,1)
151   FORMAT(' ',4X,'TOP TO LEFT',1X,I3,9X,D20.13)
      DO 152 I=1,NPX1
152   WRITE(6,153)I,SHAPE(NPX,2,I,2)
153   FORMAT(' ',4X,'TOP TO RIGHT',I3,9X,D20.13)
      WRITE(6,143)SHAPE(NPX,2,NPX,1)
      WRITE(6,144)SHAPE(NPX,1,NPX,2)
143   FORMAT(' ',4X,'TOP TO BOTTOM',11X,D20.13)
144   FORMAT(' ',4X,'BOTTOM TO TOP',11X,D20.13)
      WRITE(6,145)
145   FORMAT(///)
      RETURN
      END
//GO.SYSIN  DD *
 40199
   21
0.01D0          0.0000001D      0.0000001D0     0.0001D0
0.7D0           0.1D0
0.6D0           0.6D0           1.0D0           0.0D0
750.D0          0.01D0          1.0D0
1.0D0           1.0D0
1.0000D0        1.0000D0
```